J. Fluid Mech. (2004), *vol.* 504, *pp.* 133–165.
DOI: 10.1017/S0022112004007980 Printed in the United Kingdom

The QDIA and regularized QDIA closures for inhomogeneous turbulence over topography

By TERENCE J. O'KANE[1,2] AND JORGEN S. FREDERIKSEN[1]

[1]CSIRO Atmospheric Research, Aspendale, Victoria, Australia

[2]School of Mathematics, Monash University, Clayton, Victoria, Australia

(Received 12 September 2003 and in revised form 14 November 2003)

The dynamics and spectra of the quasi-diagonal direct interaction approximation (QDIA) closure for inhomogeneous two-dimensional turbulence over mean (single realization) topography are compared with results from direct numerical simulations (DNS). A more efficient version of the closure, termed the cumulant update QDIA (CUQDIA), has also been formulated and tested. Studies are performed for a range of resolutions, for large scale Reynolds numbers between very low ($R_L < 1$) and moderate ($R_L \approxeq 300$) and for wide ranges of topographic spectra and initial mean field and transient spectra. The QDIA-type closures are shown to be computationally tractable for general inhomogeneous flows, particularly in cumulant update form, and to perform extremely well when the turbulence is weak. At low ($R_L \approxeq 60$) to moderate ($R_L \approxeq 300$) Reynolds numbers the presence of significant amplitude small-scale mean fields and topography reduces the under-estimation of small-scale transient kinetic energy that is characteristic of the Eulerian direct interaction approximation (DIA). A regularized version of the CUQDIA closure (RCUQDIA) in which interactions are localized in wavenumber space, depending on specified cut-off ratios, has also been tested at moderate Reynolds number for cases when the small-scale mean fields and topography are weak. Excellent agreement has been found between the RCUQDIA closure and DNS results for turbulent flows with properties broadly similar to atmospheric spectra.

1. Introduction

The recent development of the quasi-diagonal direct interaction approximation closure (QDIA, Frederiksen 1999) offers the prospect of a computationally tractable means for the direct calculation of the statistics of inhomogeneous turbulence over topography. The QDIA is a generalization of the class of direct interaction approximation (DIA) theories initially developed by Kraichnan (1958, 1959; see also Leslie 1973) for isotropic turbulence. The DIA, so-called because it only takes into account directly interacting modes, has also been derived using renormalization techniques based on diagrammatic (Wyld 1961; Lee 1965), functional operator (Martin, Siggia & Rose 1973; Phythian 1975; Carnevale & Martin 1982) and path integral (Jensen 1981) formalisms.

A particular motivation for developing the QDIA closure (Frederiksen 1999) was to provide a theoretical basis for the development of subgrid scale parameterizations of eddy viscosity, stochastic backscatter and particularly the eddy-topographic force for inhomogeneous turbulent flows over topography. The eddy-topographic force describes the interaction of subgrid scale eddies with retained scale topography

and is essential for obtaining realistic ocean circulations (Holloway 1992; Alvarez *et al.* 1994). The eddy-topographic force also appears to be a missing ingredient in atmospheric general circulation models (Frederiksen, Dix & Davies 2003). However, previous attempts at a formulation were based on heuristic arguments (Holloway 1992).

Closure theories have previously been used for developing subgrid scale parameterizations for eddy viscosity and stochastic backscatter in the case of three-dimensional (e.g. Kraichnan 1976; Rose 1977; Leith 1990; Chasnov 1991; Schilling & Zhou 2002) and two-dimensional (e.g. Frederiksen and Davies 1997) homogeneous turbulence. For example, Frederiksen and Davies find that large eddy simulations (LES) incorporating eddy-damped quasi-normal Markovian (EDQNM) and DIA closure based subgrid scale parameterizations are able to maintain the same large-scale kinetic energy spectra with varying resolutions as higher resolution direct numerical simulations (DNS) of two-dimensional turbulence. Closure based dynamical subgrid scale parameterizations have also produced significant improvements in the circulation and spectra of atmospheric general circulation models (Frederiksen *et al.* 2003).

Closure theory has also traditionally been used to study the statistics of the predictability of homogeneous turbulent fluid flows in both two and three dimensions (Kraichnan 1970; Leith 1971, 1974; Leith & Kraichnan 1972). It allows the direct study of the statistics of error growth and unlike studies based on the direct numerical simulation of the primitive equations is unencumbered by issues of adequately sampling the initial error statistics (Lorenz 1969; Toth & Kalnay 1997). Of particular importance is the role of emergent coherent vorticies in quasi-two-dimensional turbulence (McWilliams 1984; Boffetta *et al.* 1997) that can have a profound effect on the predictability of geophysical flows, as evident in studies of atmospheric blocking events (see Frederiksen, Collier & Watkins 2002 and references therein). A closure model that can accurately capture the dynamics and predictability of the mean and transient statistics of general inhomogeneous flows would appear to be an important tool for the study of these types of phenomena.

The first successful attempt to incorporate random topography into a closure model for homogeneous turbulence was due to Herring (1977) dealing with ensembles of topography with zero mean value. Herring (1977) and Holloway (1978) compared both DIA and test field model (TFM) methods for the problem of two-dimensional rotating turbulent flow above a random topography. The DIA and extended TFM were found to agree qualitatively with some significant quantitative disagreement. The importance of studies of this kind, apart from developing great insight into how the statistical properties of random topography determine the spectra of transient vorticity variance, was that they enabled the identification of various spectral subranges with markedly different dynamics and showed how these subranges were influenced by the strength of the topographic amplitude relative to the convective nonlinearity (Herring 1977). However, real atmospheric and other geophysical and engineering flows tend to be inhomogeneous at the larger scales (Carnevale *et al.* 1995).

In order to examine the effect of mean topography on the structures of the inhomogeneous flows a closure theory based on single realization mean topography is required. Kraichnan (1972) formulated the DIA and TFM for general inhomogeneous turbulence interacting with mean-fields and demonstrated that the general non-diagonal form of the inhomogeneous DIA was not computationally tractable and that some form of diagonalization was required. For Boussinesq convection Kraichnan (1964*b*) developed a diagonalizing closure approximation in the special case of a mean horizontally averaged temperature field with zero fluctuations. Frederiksen

(1999) developed a quasi-diagonal DIA closure for general fields with mean and fluctuating components and applied it to inhomogeneous turbulence and mean flows over topography. The QDIA extends the family of non-Markovian statistical closures (DIA, Kraichnan 1959; self consistent field theory (SCFT), Herring 1965; local energy transfer theory (LET), McComb 1974; McComb, Filipiak & Shanmugasundaram 1992; McComb & Quinn 2003) to incorporate inhomogeneous turbulent flow over topography. These closure theories contain no arbitrary parameters but for two-dimensional turbulence have small-scale systematic biases including underestimation of small-scale kinetic energy at moderate to high Reynolds numbers (Herring *et al.* 1974; Frederiksen & Davies 2000). In particular, the Eulerian DIA produces an inertial range power law at high Reynolds number of $k^{-5/2}$, while the enstrophy cascading inertial range power law for two-dimensional turbulence is k^{-3} (Kraichnan 1964*a*; Herring *et al.* 1974).

The small-scale systematic biases of the Eulerian DIA closure arise from the fact that while the propagators, the cumulant and response functions, are renormalized there is no renormalization of the terms associated with the non-direct interactions. Martin *et al.* (1973) established the correct properties of these so-called vertex terms which in renormalized form are responsible for all information contained in the higher order cumulants. Kraichnan (1964*c*) showed that the physical foundation of the failure of the Eulerian DIA to yield the correct inertial ranges is due to its inability to distinguish between convection and intrinsic distortion effects. This means that decay times of two-time cumulant and response functions are determined incorrectly by the energy containing range rather than by local excitation levels.

A regularized form of the DIA (RDIA) containing a specified 'cut-off' parameter α which acts to localize the eddy–eddy interactions in wavenumber space has been found effective in ameliorating the small-scale deficiencies of the DIA for isotropic homogeneous turbulence (Frederiksen & Davies 2003). The physical justification for the regularization approach is the consistency with the Kolmogorov hypotheses (Kraichnan 1964*c*, 1977) and the choice of cutoff parameter seems to be, as observed in numerical experiment, almost universal (Frederiksen & Davies 2003). The RDIA corresponds to a one-parameter family of two-time non-Markovian closures just as the EDQNM (Orszag 1970, 1973; Leith 1971; Bowman, Krommes & Ottaviani 1993; Frederiksen & Davies 1997), and realizable TFM (Bowman & Krommes 1997) are one-parameter single-time Markovian models. Frederiksen & Davies (2003) show that the RDIA is in excellent agreement with DNS for two-dimensional isotropic turbulence (with $\alpha = 6$) for large-scale Reynolds numbers up to $\approxeq 4000$ and compare its performance with other closures including the TFM and quasi-Lagrangian closures (Herring & Kraichnan 1979; Gotoh, Kaneda & Bekki 1988).

The purpose of this paper is firstly to examine the performance of the QDIA closure compared with direct numerical simulation (DNS) of the barotropic vorticity equation for a range of resolutions (C3 to C64), Reynolds numbers (up to $R_L = 300$) and topographic amplitudes. The DNS and QDIA closure are both based on discrete wavenumber formulations (Frederiksen & Davies 2000) allowing unambiguous identification of intrinsic differences, although at some additional computational expense compared with continuous wavenumber formulations of the closure models. Secondly, a variant which employs a formal cumulant update procedure (CUQDIA), thereby enabling long run times, is formulated. The CUQDIA allows a significant gain in computational efficiency over the standard closure through the periodic stopping of the time integrations and calculating the two- and three-point cumulant (non-Gaussian cumulant) terms which are then used in the new initial conditions.

Finally, the regularization procedure (Frederiksen & Davies 2003) is generalized for the QDIA closure to localize eddy–mean field and eddy–topographic interactions, as well as eddy–eddy interactions, in the two-time cumulant and response functions.

In § 2 we introduce the basic equations for two-dimensional turbulent flow over topography. Then in § 3 and appendix A we introduce a method for approximating the time-history integrals which results in what we call the cumulant update QDIA (CUQDIA). In § 4 a discussion of the regularization procedure is presented after which the diagnostic quantities used in the numerical studies are defined in § 5. Section 6 briefly outlines pertinent details about the numerical methods employed to solve the closure equations as well as the barotropic vorticity equation. Detailed numerical calculations comparing the QDIA, CUQDIA and regularized CUQDIA (RCUQDIA) closures with DNS for a wide variety of topographic spectra and initial mean and transient spectra are presented in §§ 7–10. In § 7 we compare the evolution of the modal enstrophy components for both the QDIA and CUQDIA closures with DNS; we use a circular truncation with $1 \leqslant k \leqslant k_{max}$, where $k_{max} = 3$ (C3) and examine forced dissipative, viscous decaying and inviscid unforced flows. Then in § 8 the effectiveness of the quasi-diagonal approximation is demonstrated for very low large-scale Reynolds number (typically < 1) flow at resolutions C48 and C64. At such low Reynolds number the effectiveness of the quasi-diagonal approximation can be examined unencumbered by any DIA deficiencies associated with strong turbulence. Sections 9 and 10 examine the CUQDIA closure at low to moderate Reynolds number. The effect of the strength of the small-scale mean field and topographic amplitude on the accuracy of the closure is investigated for turbulent flow at C48 and C64 resolutions. We investigate the performance of the CUQDIA closure in reproducing evolved DNS kinetic energy, palinstrophy, large-scale Reynolds number and skewness. In § 10, the performance of the RCUQDIA closure is also compared with both DNS and CUQDIA results for two particular choices of cutoff parameters. Finally in § 11 we discuss the implications of our results and summarize our conclusions.

2. Two-dimensional flow on a f-plane

The evolution of two-dimensional flow over a mean topography on a periodic f-plane ($0 \leqslant x \leqslant 2\pi$), ($0 \leqslant y \leqslant 2\pi$) is described by the barotropic vorticity equation

$$\frac{\partial \zeta}{\partial t} = -J(\psi, \zeta + h) + \nu_0 \nabla^2 \zeta + f^0, \tag{2.1a}$$

where f^0 is the bare forcing and ν_0 the bare viscosity, and

$$J(\psi, \zeta) = \frac{\partial \psi}{\partial x}\frac{\partial \zeta}{\partial y} - \frac{\partial \psi}{\partial y}\frac{\partial \zeta}{\partial x} \tag{2.1b}$$

is the Jacobian. The vorticity is the Laplacian of the streamfunction, i.e. $\zeta = \nabla^2 \psi$. We assume that the variation in the topography (ΔH) is small, and define h to be the scaled spatial variation of the height of the topography relative to the total depth. The barotropic vorticity equation can be made non-dimensional by introducing suitable length and time scales.

The vorticity equation, and subsequent closure equations, are most conveniently analysed and solved in spectral space. We expand each of the functions in a Fourier series; for example

$$\zeta(\boldsymbol{x}, t) = \sum_{\boldsymbol{k}} \zeta_{\boldsymbol{k}}(t) \exp(\mathrm{i}\boldsymbol{k} \cdot \boldsymbol{x}), \tag{2.2a}$$

where

$$\zeta_{\boldsymbol{k}}(t) = \frac{1}{(2\pi)^2}\int_0^{2\pi} \mathrm{d}^2\boldsymbol{x}\,\zeta(\boldsymbol{x},t)\exp(-\mathrm{i}\boldsymbol{k}\cdot\boldsymbol{x}) \tag{2.2b}$$

and $\boldsymbol{x}=(x,y)$, $\boldsymbol{k}=(k_x,k_y)$. The spectral vorticity equation with a more general dissipation where $\nu_0 \to \nu_0(k)$ then takes the form

$$\left(\frac{\partial}{\partial t}+\nu_0(k)k^2\right)\zeta_{\boldsymbol{k}}(t) = \sum_{\boldsymbol{p}}\sum_{\boldsymbol{q}}\delta(\boldsymbol{k}+\boldsymbol{p}+\boldsymbol{q})[K(\boldsymbol{k},\boldsymbol{p},\boldsymbol{q})\zeta_{-\boldsymbol{p}}\zeta_{-\boldsymbol{q}} + A(\boldsymbol{k},\boldsymbol{p},\boldsymbol{q})\zeta_{-\boldsymbol{p}}h_{-\boldsymbol{q}}] + f_{\boldsymbol{k}}^0, \tag{2.3}$$

where $k=(k_x^2+k_y^2)^{1/2}$ and $\zeta_{-\boldsymbol{k}}$ is conjugate to $\zeta_{\boldsymbol{k}}$. The interaction coefficients are defined by relationships

$$A(\boldsymbol{k},\boldsymbol{p},\boldsymbol{q}) = -(p_xq_y - p_yq_x)/p^2, \tag{2.4a}$$

$$K(\boldsymbol{k},\boldsymbol{p},\boldsymbol{q}) = \tfrac{1}{2}[A(\boldsymbol{k},\boldsymbol{p},\boldsymbol{q}) + A(\boldsymbol{k},\boldsymbol{q},\boldsymbol{p})] = \tfrac{1}{2}(p_xq_y - p_yq_x)(p^2-q^2)/p^2q^2, \tag{2.4b}$$

where

$$\delta(\boldsymbol{k}+\boldsymbol{p}+\boldsymbol{q}) = \begin{cases} 1 & \text{if } \boldsymbol{k}+\boldsymbol{p}+\boldsymbol{q}=0, \\ 0 & \text{otherwise} \end{cases} \tag{2.4c}$$

and we note that

$$K(\boldsymbol{k},\boldsymbol{p},\boldsymbol{q}) + K(\boldsymbol{p},\boldsymbol{q},\boldsymbol{k}) + K(\boldsymbol{q},\boldsymbol{k},\boldsymbol{p}) = 0. \tag{2.4d}$$

For the purposes of this paper the topography is represented in the form

$$h_{\boldsymbol{k}} = |h_{\boldsymbol{k}}| \times (\cos\theta_{\boldsymbol{k}} + \mathrm{i}\sin\theta_{\boldsymbol{k}}) \tag{2.5}$$

with $\theta_{\boldsymbol{k}}$ a fixed specified random phase. For an ensemble of flows satisfying (2.3), we may express the vorticity $\zeta_{\boldsymbol{k}}$ and forcing $f_{\boldsymbol{k}}^0$ in terms of their ensemble means, denoted by $\langle\rangle$, and the deviations from the ensemble mean, denoted by $\hat{}$:

$$\zeta_{\boldsymbol{k}} = \langle\zeta_{\boldsymbol{k}}\rangle + \hat{\zeta}_{\boldsymbol{k}}, \tag{2.6a}$$

$$f_{\boldsymbol{k}}^0 = \langle f_{\boldsymbol{k}}^0\rangle + \hat{f_{\boldsymbol{k}}^0}. \tag{2.6b}$$

The equations for the ensemble mean and the deviation can then be written in the form:

$$\left(\frac{\partial}{\partial t}+\nu_0(k)k^2\right)\langle\zeta_{\boldsymbol{k}}\rangle = \sum_{\boldsymbol{p}}\sum_{\boldsymbol{q}}\delta(\boldsymbol{k}+\boldsymbol{p}+\boldsymbol{q})K(\boldsymbol{k},\boldsymbol{p},\boldsymbol{q})[\langle\zeta_{-\boldsymbol{p}}\rangle\langle\zeta_{-\boldsymbol{q}}\rangle + C_{-\boldsymbol{p},-\boldsymbol{q}}(t,t)] + \sum_{\boldsymbol{p}}\sum_{\boldsymbol{q}}\delta(\boldsymbol{k}+\boldsymbol{p}+\boldsymbol{q})A(\boldsymbol{k},\boldsymbol{p},\boldsymbol{q})\langle\zeta_{-\boldsymbol{p}}\rangle h_{-\boldsymbol{q}} + \langle f_{\boldsymbol{k}}^0\rangle \tag{2.7a}$$

$$\left(\frac{\partial}{\partial t}+\nu_0(k)k^2\right)\hat{\zeta}_{\boldsymbol{k}} = \sum_{\boldsymbol{p}}\sum_{\boldsymbol{q}}\delta(\boldsymbol{k}+\boldsymbol{p}+\boldsymbol{q})K(\boldsymbol{k},\boldsymbol{p},\boldsymbol{q}) \times [\langle\zeta_{-\boldsymbol{p}}\rangle\hat{\zeta}_{-\boldsymbol{q}} + \hat{\zeta}_{-\boldsymbol{p}}\langle\zeta_{-\boldsymbol{q}}\rangle + \hat{\zeta}_{-\boldsymbol{p}}\hat{\zeta}_{-\boldsymbol{q}} - C_{-\boldsymbol{p},-\boldsymbol{q}}(t,t)] + \sum_{\boldsymbol{p}}\sum_{\boldsymbol{q}}\delta(\boldsymbol{k}+\boldsymbol{p}+\boldsymbol{q})A(\boldsymbol{k},\boldsymbol{p},\boldsymbol{q})\hat{\zeta}_{-\boldsymbol{p}}h_{-\boldsymbol{q}} + \hat{f}_{\boldsymbol{k}}^0. \tag{2.7b}$$

Here the two-point cumulant is defined by

$$C_{-\boldsymbol{p},-\boldsymbol{q}}(t,s) = \langle\hat{\zeta}_{-\boldsymbol{p}}(t)\hat{\zeta}_{-\boldsymbol{q}}(s)\rangle. \tag{2.8}$$

3. QDIA and cumulant update QDIA closure equations

The quasi-diagonal DIA closure equations (QDIA, Frederiksen 1999) were derived on the basis that the perturbation fields $\hat{\zeta}_{\boldsymbol{k}}$ have, to lowest order, a multivariate Gaussian distribution. This allows the representation of the off-diagonal two-point cumulant and response functions in terms of the diagonal elements. The resulting equations for the mean field, two-point cumulant and response functions are expressed entirely in terms of the diagonal elements of the two-point cumulant and response functions and are computationally much more efficient than the general inhomogeneous closure equations (Kraichnan 1972). However, the QDIA like other non-Markovian closure theories, may be computationally expensive for long time-integrations because of the time-history integrals which need to be evaluated between the initial and final times. This makes it desirable to implement a generalization of the cumulant update restart procedure used by Rose (1985), Frederiksen, Davies & Bell (1994) and Frederiksen & Davies (2000, 2003).

Our cumulant update restart procedure consists of integrating the QDIA forward for a time, calculating the two- and three-point terms at this time and then using these in the new initial conditions for further integration. In principle, knowledge of all higher order cumulants should be available, but to be consistent with the approximations of the QDIA, only the two- and three-point cumulants are needed. The crucial information contained in the three-point term is that of the non-Gaussian cumulants accumulated in the time-history integrals. The three-point cumulant is effectively the homogeneous component of the closure equations while the two-point terms arise due to the inhomogeneity produced by the presence of topography and mean field. In Appendix A we present a derivation of the two-point restart terms while the method of deriving the three-point terms follows that used by Rose (1985) & Frederiksen *et al.* (1994).

The basis of the QDIA closure is the representation of the off-diagonal elements of the two- and three-point cumulant and response functions in terms of the diagonal elements. Following Frederiksen (1999) we have

$$\begin{aligned} C_{\boldsymbol{k},-\boldsymbol{l}}(t,t') = &\int_{t_0}^{t} \mathrm{d}s\, R_{\boldsymbol{k}}(t,s) C_{\boldsymbol{l}}(s,t') \left[A(\boldsymbol{k},-\boldsymbol{l},\boldsymbol{l}-\boldsymbol{k}) h_{(\boldsymbol{k}-\boldsymbol{l})} + 2K(\boldsymbol{k},-\boldsymbol{l},\boldsymbol{l}-\boldsymbol{k}) \left\langle \zeta_{(\boldsymbol{k}-\boldsymbol{l})}(s) \right\rangle \right] \\ &+ \int_{t_0}^{t'} \mathrm{d}s\, R_{-\boldsymbol{l}}(t',s) C_{\boldsymbol{k}}(t,s) \left[A(-\boldsymbol{l},\boldsymbol{k},\boldsymbol{l}-\boldsymbol{k}) h_{(\boldsymbol{k}-\boldsymbol{l})} \right. \\ &\left. + 2K(-\boldsymbol{l},\boldsymbol{k},\boldsymbol{l}-\boldsymbol{k}) \left\langle \zeta_{(\boldsymbol{k}-\boldsymbol{l})}(s) \right\rangle \right] + R_{\boldsymbol{k}}(t,t_0) R_{-\boldsymbol{l}}(t',t_0) \tilde{K}^{(2)}_{\boldsymbol{k},-\boldsymbol{l}}(t_0,t_0), \end{aligned} \tag{3.1a}$$

where $\tilde{K}^{(2)}_{\boldsymbol{k},-\boldsymbol{l}}(t_0,t_0)$ is the contribution to the off-diagonal covariance matrix at initial time t_0. The treatment of the three-point cumulant is the same as in the DIA closure for homogeneous turbulence (Kraichnan 1959; Frederiksen & Davies 2000):

$$\begin{aligned} \left\langle \hat{\zeta}_{-\boldsymbol{l}}(t) \hat{\zeta}_{(\boldsymbol{l}-\boldsymbol{k})}(t) \hat{\zeta}_{\boldsymbol{k}}(t') \right\rangle = &2 \int_{t_0}^{t'} \mathrm{d}s\, K(\boldsymbol{k},-\boldsymbol{l},\boldsymbol{l}-\boldsymbol{k}) C_{-\boldsymbol{l}}(t,s) C_{(\boldsymbol{l}-\boldsymbol{k})}(t,s) R_{\boldsymbol{k}}(t',s) \\ &+ 2 \int_{t_0}^{t} \mathrm{d}s\, K(-\boldsymbol{l},\boldsymbol{l}-\boldsymbol{k},\boldsymbol{k}) R_{-\boldsymbol{l}}(t,s) C_{(\boldsymbol{l}-\boldsymbol{k})}(t,s) C_{\boldsymbol{k}}(t',s) \\ &+ 2 \int_{t_0}^{t} \mathrm{d}s\, K(\boldsymbol{l}-\boldsymbol{k},-\boldsymbol{l},\boldsymbol{k}) R_{(\boldsymbol{l}-\boldsymbol{k})}(t,s) C_{-\boldsymbol{l}}(t,s) C_{\boldsymbol{k}}(t',s) \\ &+ R_{-\boldsymbol{l}}(t,t_0) R_{(\boldsymbol{l}-\boldsymbol{k})}(t,t_0) R_{\boldsymbol{k}}(t,t_0) \tilde{K}^{(3)}_{-\boldsymbol{l},(\boldsymbol{l}-\boldsymbol{k}),\boldsymbol{k}}(t_0,t_0,t_0), \end{aligned} \tag{3.1b}$$

where $\tilde{K}^{(3)}_{-\boldsymbol{l},(\boldsymbol{l}-\boldsymbol{k}),\boldsymbol{k}}(t_0,t_0,t_0)$ allows for non-Gaussian initial conditions. Similarly, the response function is given by

$$R_{\boldsymbol{k},\boldsymbol{l}}(t,t') = \int_{t'}^{t} \mathrm{d}s\, R_{\boldsymbol{k}}(t,s)R_{\boldsymbol{l}}(s,t') \times \left[A(\boldsymbol{k},-\boldsymbol{l},\boldsymbol{l}-\boldsymbol{k})h_{(\boldsymbol{k}-\boldsymbol{l})} + 2K(\boldsymbol{k},-\boldsymbol{l},\boldsymbol{l}-\boldsymbol{k})\left\langle\zeta_{(\boldsymbol{k}-\boldsymbol{l})}(s)\right\rangle\right]. \quad (3.1c)$$

Here

$$R_{\boldsymbol{k},\boldsymbol{l}}(t,t') = \left\langle \frac{\delta\hat{\zeta}_{\boldsymbol{k}}(t)}{\delta\hat{f}^0_{\boldsymbol{l}}(t')}\right\rangle, \quad (3.2a)$$

and we use the abbreviations

$$C_{\boldsymbol{k}}(t,t') = C_{\boldsymbol{k},-\boldsymbol{k}}(t,t'); \qquad R_{\boldsymbol{k}}(t,t') = R_{\boldsymbol{k},\boldsymbol{k}}(t,t'). \quad (3.2b)$$

Then, using (3.1a) in (2.7a), the mean-field equation takes the form

$$\left(\frac{\partial}{\partial t} + \nu_0(k)k^2\right)\langle\zeta_{\boldsymbol{k}}\rangle = \sum_{\boldsymbol{p}}\sum_{\boldsymbol{q}} \delta(\boldsymbol{k}+\boldsymbol{p}+\boldsymbol{q})[K(\boldsymbol{k},\boldsymbol{p},\boldsymbol{q})\langle\zeta_{-\boldsymbol{p}}(t)\rangle\langle\zeta_{-\boldsymbol{q}}(t)\rangle + A(\boldsymbol{k},\boldsymbol{p},\boldsymbol{q})\langle\zeta_{-\boldsymbol{p}}(t)\rangle h_{-\boldsymbol{q}}] - \int_{t_0}^{t}\mathrm{d}s\,\eta_{\boldsymbol{k}}(t,s)\langle\zeta_{\boldsymbol{k}}(s)\rangle + h_{\boldsymbol{k}}\int_{t_0}^{t}\mathrm{d}s\,\chi_{\boldsymbol{k}}(t,s) + \left\langle f^0_{\boldsymbol{k}}(t)\right\rangle + \sum_{\boldsymbol{p}}\sum_{\boldsymbol{q}}\delta(\boldsymbol{k}+\boldsymbol{p}+\boldsymbol{q}) \times K(\boldsymbol{k},\boldsymbol{p},\boldsymbol{q})\tilde{K}^{(2)}_{-\boldsymbol{p},-\boldsymbol{q}}(t_0,t_0)R_{-\boldsymbol{p}}(t,t_0)R_{-\boldsymbol{q}}(t,t_0). \quad (3.3)$$

Here, the nonlinear damping

$$\eta_{\boldsymbol{k}}(t,s) = -4\sum_{\boldsymbol{p}}\sum_{\boldsymbol{q}}\delta(\boldsymbol{k}+\boldsymbol{p}+\boldsymbol{q})K(\boldsymbol{k},\boldsymbol{p},\boldsymbol{q})K(-\boldsymbol{p},-\boldsymbol{q},-\boldsymbol{k})R_{-\boldsymbol{p}}(t,s)C_{-\boldsymbol{q}}(t,s), \quad (3.4a)$$

measures the interaction of transient eddies with the mean field while

$$\chi_{\boldsymbol{k}}(t,s) = 2\sum_{\boldsymbol{p}}\sum_{\boldsymbol{q}}\delta(\boldsymbol{k}+\boldsymbol{p}+\boldsymbol{q})K(\boldsymbol{k},\boldsymbol{p},\boldsymbol{q})A(-\boldsymbol{p},-\boldsymbol{q},-\boldsymbol{k})R_{-\boldsymbol{p}}(t,s)C_{-\boldsymbol{q}}(t,s), \quad (3.4b)$$

measures the strength of the interaction of transient eddies with the topography in (3.3).

The equation for the diagonal two-time two-point cumulant is obtained by multiplying (2.7b) by $\hat{\zeta}_{-\boldsymbol{k}}(t')$ and using (3.1a) and (3.1b):

$$\left(\frac{\partial}{\partial t} + \nu_0(k)k^2\right)C_{\boldsymbol{k}}(t,t') = N_{\boldsymbol{k}}(t,t'), \quad (3.5)$$

where

$$N_{\boldsymbol{k}}(t,t') = \int_{t_0}^{t'}\mathrm{d}s\left[S_{\boldsymbol{k}}(t,s)+P_{\boldsymbol{k}}(t,s)+F^0_{\boldsymbol{k}}(t,s)\right]R_{-\boldsymbol{k}}(t',s) - \int_{t_0}^{t}\mathrm{d}s\,[\eta_{\boldsymbol{k}}(t,s)+\pi_{\boldsymbol{k}}(t,s)] \times C_{-\boldsymbol{k}}(t',s) + \sum_{\boldsymbol{p}}\sum_{\boldsymbol{q}}\delta(\boldsymbol{k}+\boldsymbol{p}+\boldsymbol{q})K(\boldsymbol{k},\boldsymbol{p},\boldsymbol{q})\tilde{K}^{(3)}_{-\boldsymbol{q},-\boldsymbol{p},-\boldsymbol{k}}(t_0,t_0,t_0) \times R_{-\boldsymbol{q}}(t,t_0)R_{-\boldsymbol{p}}(t,t_0)R_{-\boldsymbol{k}}(t',t_0) + \sum_{\boldsymbol{p}}\sum_{\boldsymbol{q}}\delta(\boldsymbol{k}+\boldsymbol{p}+\boldsymbol{q})[(A(\boldsymbol{k},\boldsymbol{p},\boldsymbol{q}) + A(\boldsymbol{k},\boldsymbol{q},\boldsymbol{p}))\langle\zeta_{-\boldsymbol{q}}(t)\rangle + A(\boldsymbol{k},\boldsymbol{p},\boldsymbol{q})h_{-\boldsymbol{q}}] \times \tilde{K}^{(2)}_{-\boldsymbol{p},-\boldsymbol{k}}(t_0,t_0)R_{-\boldsymbol{p}}(t,t_0)R_{-\boldsymbol{k}}(t',t_0). \quad (3.6)$$

Here

$$F_{\boldsymbol{k}}^{0}(t,s)=\left\langle \hat{f}_{\boldsymbol{k}}^{0}(t)\hat{f}_{\boldsymbol{k}}^{0*}(s)\right\rangle \tag{3.7a}$$

is the variance of the random forcing,

$$S_{\boldsymbol{k}}(t,s)=2\sum_{\boldsymbol{p}}\sum_{\boldsymbol{q}}\delta(\boldsymbol{k}+\boldsymbol{p}+\boldsymbol{q})K(\boldsymbol{k},\boldsymbol{p},\boldsymbol{q})K(-\boldsymbol{k},-\boldsymbol{p},-\boldsymbol{q})C_{-\boldsymbol{p}}(t,s)C_{-\boldsymbol{q}}(t,s), \tag{3.7b}$$

is the nonlinear noise and

$$\begin{aligned}P_{\boldsymbol{k}}(t,s)=&\sum_{\boldsymbol{p}}\sum_{\boldsymbol{q}}\delta(\boldsymbol{k}+\boldsymbol{p}+\boldsymbol{q})C_{-\boldsymbol{p}}(t,s)[(A(\boldsymbol{k},\boldsymbol{p},\boldsymbol{q})+A(\boldsymbol{k},\boldsymbol{q},\boldsymbol{p}))\langle\zeta_{-\boldsymbol{q}}(t)\rangle+A(\boldsymbol{k},\boldsymbol{p},\boldsymbol{q})h_{-\boldsymbol{q}}]\\&\times[(A(-\boldsymbol{k},-\boldsymbol{p},-\boldsymbol{q})+A(-\boldsymbol{k},-\boldsymbol{q},-\boldsymbol{p}))\langle\zeta_{\boldsymbol{q}}(s)\rangle+A(-\boldsymbol{k},-\boldsymbol{p},-\boldsymbol{q})h_{\boldsymbol{q}}],\end{aligned} \tag{3.7c}$$

$$\begin{aligned}\pi_{\boldsymbol{k}}(t,s)=&-\sum_{\boldsymbol{p}}\sum_{\boldsymbol{q}}\delta(\boldsymbol{k}+\boldsymbol{p}+\boldsymbol{q})R_{-\boldsymbol{p}}(t,s)[(A(\boldsymbol{k},\boldsymbol{p},\boldsymbol{q})+A(\boldsymbol{k},\boldsymbol{q},\boldsymbol{p}))\langle\zeta_{-\boldsymbol{q}}(t)\rangle+A(\boldsymbol{k},\boldsymbol{p},\boldsymbol{q})h_{-\boldsymbol{q}}]\\&\times[(A(-\boldsymbol{p},-\boldsymbol{k},-\boldsymbol{q})+A(-\boldsymbol{p},-\boldsymbol{q},-\boldsymbol{k}))\langle\zeta_{\boldsymbol{q}}(s)\rangle+A(-\boldsymbol{p},-\boldsymbol{k},-\boldsymbol{q})h_{\boldsymbol{q}}],\end{aligned} \tag{3.7d}$$

are noise and dissipation terms associated with eddy-mean field and eddy-topographic interactions. In these latter terms we have used (2.4*b*) to express the $K(\boldsymbol{k},\boldsymbol{p},\boldsymbol{q})$ interaction coefficient in terms of $A(\boldsymbol{k},\boldsymbol{p},\boldsymbol{q})$ and $A(\boldsymbol{k},\boldsymbol{q},\boldsymbol{p})$ for later convenience when we consider the regularization of the interaction coefficients. Equations (3.5) and (3.6) generalize the QDIA closure of Frederiksen (1999) by including initial contributions to the off-diagonal covariance matrix ($\tilde{K}^{(2)}_{-\boldsymbol{p},-\boldsymbol{k}}(t_0,t_0)$) and to non-Gaussian initial conditions associated with the three-point function ($\tilde{K}^{(3)}_{-\boldsymbol{q},-\boldsymbol{p},-\boldsymbol{k}}(t_0,t_0,t_0)$).

The equation for the diagonal response function is obtained by using (3.1*c*) as in Frederiksen (1999):

$$\left(\frac{\partial}{\partial t}+\nu_0(k)k^2\right)R_{\boldsymbol{k}}(t,t')=-\int_{t'}^{t}\mathrm{d}s\,[\eta_{\boldsymbol{k}}(t,s)+\pi_{\boldsymbol{k}}(t,s)]\,R_{\boldsymbol{k}}(s,t'), \tag{3.8}$$

with $R_{\boldsymbol{k}}(t,t)=1$ and for $t<t'$ we have $R_{\boldsymbol{k}}(t,t')=0$. The equation for the diagonal single-time two-point cumulant is

$$\left(\frac{\partial}{\partial t}+2\nu_0(k)k^2\right)C_{\boldsymbol{k}}(t,t)=2\mathrm{Re}\;N_{\boldsymbol{k}}(t,t) \tag{3.9a}$$

since

$$\frac{\partial C_{\boldsymbol{k}}(t,t)}{\partial t}=\lim_{t'\to t}\left(\frac{\partial C_{\boldsymbol{k}}(t,t')}{\partial t}+\frac{\partial C_{\boldsymbol{k}}(t,t')}{\partial t'}\right) \tag{3.9b}$$

and $C_{\boldsymbol{k}}(t',t)=C_{-\boldsymbol{k}}(t,t')=C^{*}_{\boldsymbol{k}}(t,t')$.

These QDIA closure equations, including off-diagonal and non-Gaussian initial conditions may then be used to periodically truncate the potentially long time-history integrals and obtain a more efficient closure scheme which we call the cumulant update QDIA (CUQDIA). The method relies on the fact that the essential information contained in the time-history integrals is the off-diagonal two-point cumulant and the three-point cumulant. Suppose we integrate the QDIA closure equations from the initial time $t_0=0$ up to a time $t'=t=T$. Then the off-diagonal two-point cumulant

and the three-point cumulant may be calculated through the relationships

$$\tilde{K}^{(2)}_{-\boldsymbol{p},-\boldsymbol{k}}(T,T) = K^{(2)Dyn}_{-\boldsymbol{p},-\boldsymbol{k}}(T,T) + \tilde{K}^{(2)}_{-\boldsymbol{p},-\boldsymbol{k}}(t_0,t_0)R_{-\boldsymbol{p}}(T,t_0)R_{-\boldsymbol{k}}(T,t_0), \tag{3.10a}$$

$$\tilde{K}^{(3)}_{-\boldsymbol{q},-\boldsymbol{p},-\boldsymbol{k}}(T,T,T) = K^{(3)Dyn}_{-\boldsymbol{q},-\boldsymbol{p},-\boldsymbol{k}}(T,T,T) + \tilde{K}^{(3)}_{-\boldsymbol{q},-\boldsymbol{p},-\boldsymbol{k}}(t_0,t_0,t_0)R_{-\boldsymbol{q}}(T,t_0)R_{-\boldsymbol{p}}(T,t_0)R_{-\boldsymbol{k}}(T,t_0). \tag{3.10b}$$

Here

$$\begin{aligned} K^{(2)Dyn}_{-\boldsymbol{p},-\boldsymbol{k}}(t,t') = \int_{t_0}^{t} \mathrm{d}s\, R_{-\boldsymbol{p}}(t,s)C_{-\boldsymbol{k}}(t',s)\big[&A(-\boldsymbol{p},-\boldsymbol{k},\boldsymbol{k}+\boldsymbol{p})h_{(-\boldsymbol{k}-\boldsymbol{p})} \\ &+ (A(-\boldsymbol{p},-\boldsymbol{k},\boldsymbol{k}+\boldsymbol{p}) + A(-\boldsymbol{p},\boldsymbol{k}+\boldsymbol{p},-\boldsymbol{k}))\big\langle\zeta_{(-\boldsymbol{k}-\boldsymbol{p})}(s)\big\rangle\big] \\ + \int_{t_0}^{t'} \mathrm{d}s\, R_{-\boldsymbol{k}}(t',s)C_{-\boldsymbol{p}}(t,s)\big[&A(-\boldsymbol{k},-\boldsymbol{p},\boldsymbol{k}+\boldsymbol{p})h_{(-\boldsymbol{k}-\boldsymbol{p})} \\ &+ (A(-\boldsymbol{k},-\boldsymbol{p},\boldsymbol{k}+\boldsymbol{p}) + A(-\boldsymbol{k},\boldsymbol{k}+\boldsymbol{p},-\boldsymbol{p}))\big\langle\zeta_{(-\boldsymbol{k}-\boldsymbol{p})}(s)\big\rangle\big], \end{aligned} \tag{3.11a}$$

$$\sum_{\boldsymbol{p}}\sum_{\boldsymbol{q}} \delta(\boldsymbol{k}+\boldsymbol{p}+\boldsymbol{q})K(\boldsymbol{k},\boldsymbol{p},\boldsymbol{q})K^{(3)Dyn}_{-\boldsymbol{q},-\boldsymbol{p},-\boldsymbol{k}}(t,t,t') = \int_{t_0}^{t'} \mathrm{d}s\, S_{\boldsymbol{k}}(t,s)R_{-\boldsymbol{k}}(t',s) - \int_{t_0}^{t} \mathrm{d}s\, \eta_{\boldsymbol{k}}(t,s)C_{-\boldsymbol{k}}(t',s). \tag{3.11b}$$

and $K^{(2)Dyn}$ also satisfies the sum rules

$$\sum_{\boldsymbol{p}}\sum_{\boldsymbol{q}} \delta(\boldsymbol{k}+\boldsymbol{p}+\boldsymbol{q})K(\boldsymbol{k},\boldsymbol{p},\boldsymbol{q})K^{(2)Dyn}_{-\boldsymbol{p},-\boldsymbol{q}}(t,t) = -\int_{t_0}^{t} \mathrm{d}s\, \eta_{\boldsymbol{k}}(t,s)\langle\zeta_{\boldsymbol{k}}(s)\rangle + h_{\boldsymbol{k}}\int_{t_0}^{t} \mathrm{d}s\, \chi_{\boldsymbol{k}}(t,s) \tag{3.11c}$$

and

$$\sum_{\boldsymbol{p}}\sum_{\boldsymbol{q}} \delta(\boldsymbol{k}+\boldsymbol{p}+\boldsymbol{q})[(A(\boldsymbol{k},\boldsymbol{p},\boldsymbol{q}) + A(\boldsymbol{k},\boldsymbol{q},\boldsymbol{p}))\langle\zeta_{-\boldsymbol{q}}(t)\rangle + A(\boldsymbol{k},\boldsymbol{p},\boldsymbol{q})h_{-\boldsymbol{q}}] \times \tilde{K}^{(2)Dyn}_{-\boldsymbol{p},-\boldsymbol{k}}(t,t') = \int_{t_0}^{t'} \mathrm{d}s\, P_{\boldsymbol{k}}(t,s)R_{-\boldsymbol{k}}(t',s) - \int_{t_0}^{t} \mathrm{d}s\, \pi_{\boldsymbol{k}}(t,s)C_{-\boldsymbol{k}}(t',s). \tag{3.11d}$$

Equations (3.10) and (3.11) follow from consistency with (3.3), (3.5) and (3.6). The procedure may then be performed as often as required by simply replacing $\tilde{K}^{(2)}_{-\boldsymbol{p},-\boldsymbol{k}}(t_0,t_0)$, $\tilde{K}^{(2)}_{-\boldsymbol{p},-\boldsymbol{q}}(t_0,t_0)$ and $\tilde{K}^{(3)}_{-\boldsymbol{q},-\boldsymbol{p},-\boldsymbol{k}}(t_0,t_0,t_0)$ with the quantities $\tilde{K}^{(2)}_{-\boldsymbol{p},-\boldsymbol{k}}(T,T)$, $\tilde{K}^{(2)}_{-\boldsymbol{p},-\boldsymbol{q}}(T,T)$ and $\tilde{K}^{(3)}_{-\boldsymbol{q},-\boldsymbol{p},-\boldsymbol{k}}(T,T,T)$.

The QDIA closure equations conserve kinetic energy and potential enstrophy (in the absence of forcing and dissipation) and guarantee realizability for the diagonal elements of the covariance matrices (Frederiksen 1999).

4. Regularization

The Eulerian DIA (for homogeneous isotropic turbulence) produces kinetic energy spectra that closely match those of DNS in the energy containing range of large scales (e.g. Herring *et al.* 1974; Frederiksen & Davies 2003). However, at high Reynolds number the Eulerian DIA results in power laws that differ slightly from the

Kolmogorov inertial range power laws. Kraichnan (1964*a*) showed that this problem is due to the fact that the DIA does not distinguish between convection effects and intrinsic distortion effects. He also examined a number of ways of modifying the DIA to yield the Kolmogorov spectra. One method, which has recently been examined by Frederiksen & Davies (2003) for two-dimensional isotropic turbulence, consists of zeroing the interaction coefficient in the two-time cumulant and response function equations unless the triad of interacting wave vectors satisfy certain inequalities that localize the transfers and that depend on a cut-off ratio α (defined by (4.1*a*)). Frederiksen & Davies (2003) called this method regularization because it removes the low wavenumber divergence of the DIA response function when a Kolmogorov spectrum is assumed (Leslie 1973; McComb 1990).

The RDIA approximates the inclusion of non-direct interactions; it corresponds to a simple empirical vertex renormalization depending on the parameter α, and in this respect is similar to the TFM (Kraichnan 1971*a*,*b*; Herring 1977). However, the RDIA correctly represents the two-time cumulant properties in contrast to the single-time Markovian TFM. Frederiksen & Davies (2003) compared the RDIA with ensemble-averaged direct numerical simulations (DNS) for decaying two-dimensional turbulence at large-scale Reynolds numbers up to 4000. They considered discrete wavenumber representations relevant to flows on the doubly periodic plane, focusing on the evolved kinetic energy, enstrophy, palinstrophy and enstrophy flux spectra as well as skewness evolution. All diagnostics were shown to compare well with DNS for $\alpha = 6$ which was found to be almost universal.

In the case of isotropic turbulence (Frederiksen & Davies 2003), the regularization consists of zeroing the interaction coefficient $K(\boldsymbol{k}, \boldsymbol{p}, \boldsymbol{q})$ (2.4*b*) if $p < k/\alpha$ or $q < k/\alpha$ in the two-time cumulant and response function equations of the DIA closure. That is, in these two-time equations $K(\boldsymbol{k}, \boldsymbol{p}, \boldsymbol{q})$ is replaced by

$$\Theta\left(p - \frac{k}{\alpha_1}\right)\Theta\left(q - \frac{k}{\alpha_1}\right)K(\boldsymbol{k}, \boldsymbol{p}, \boldsymbol{q}), \tag{4.1a}$$

where $\alpha_1 = \alpha$. The interaction coefficient is unchanged in the single-time cumulant equation. In the present case of inhomogeneous turbulence over topography we also need to consider the $A(\boldsymbol{k}, \boldsymbol{p}, \boldsymbol{q})$ interaction coefficient. This is replaced by

$$\Theta\left(p - \frac{k}{\alpha_2}\right)\Theta\left(q - \frac{k}{\alpha_2}\right)A(\boldsymbol{k}, \boldsymbol{p}, \boldsymbol{q}). \tag{4.1b}$$

in the two-time cumulant and response function equations while $K(\boldsymbol{k}, \boldsymbol{p}, \boldsymbol{q})$ is again replaced by the expression in (4.1*a*). We shall explore cases when α_1 and α_2 are different and when they take the same value. Again, the interaction coefficients are unchanged in the single-time cumulant equation and in the mean-field equation.

The regularization of the $A(\boldsymbol{k}, \boldsymbol{p}, \boldsymbol{q})$ interaction coefficient results in a localization of the eddy-mean field and eddy-topographic transfers, just as the regularization of the $K(\boldsymbol{k}, \boldsymbol{p}, \boldsymbol{q})$ interaction coefficient ensures that transfer from large to small scales proceeds by a cascade that is local in wavenumber (Kraichnan 1964*c*). We expect, and confirm, that at reasonable Reynolds numbers the localization of the eddy-mean field and eddy-topographic transfers, as well as of the eddy-eddy transfers, is necessary for the QDIA spectra to compare closely with DNS results at high wavenumbers.

5. Diagnostics

In the sections that follow prognostic DNS and closure equations are analysed using the following diagnostics for the kinetic energy and palinstrophy

$$\mathscr{E}(t) = \tfrac{1}{2}\sum_{\boldsymbol{k}}[C_{\boldsymbol{k}}(t,t) + \langle\zeta_{\boldsymbol{k}}(t)\rangle\langle\zeta_{-\boldsymbol{k}}(t)\rangle]/k^2, \tag{5.1a}$$

$$\mathscr{P}(t) = \tfrac{1}{2}\sum_{\boldsymbol{k}}[C_{\boldsymbol{k}}(t,t) + \langle\zeta_{\boldsymbol{k}}(t)\rangle\langle\zeta_{-\boldsymbol{k}}(t)\rangle]k^2. \tag{5.1b}$$

The components defined in (5.1) are used to calculate band-averaged spectra defined as

$$E(k_i,t) = \tfrac{1}{2}\sum_{\boldsymbol{k}\in S}[C_{\boldsymbol{k}}(t,t) + \langle\zeta_{\boldsymbol{k}}(t)\rangle\langle\zeta_{-\boldsymbol{k}}(t)\rangle]/k^2, \tag{5.2a}$$

$$P(k_i,t) = \tfrac{1}{2}\sum_{\boldsymbol{k}\in S}[C_{\boldsymbol{k}}(t,t) + \langle\zeta_{\boldsymbol{k}}(t)\rangle\langle\zeta_{-\boldsymbol{k}}(t)\rangle]k^2. \tag{5.2b}$$

The set S is defined as

$$S = \left[\boldsymbol{k}|k_i = \mathrm{Int}\left[k + \tfrac{1}{2}\right]\right] \tag{5.3}$$

where the subscript i indicates that the integer part is taken in (5.3) so that all $\boldsymbol{k}$ that lie within a given radius band of unit width are summed over.

In all calculations to follow the more general viscosity $\nu_0(k)$ is replaced by the non-dimensional viscosity $\hat{\nu}$. We then define the palinstrophy production and enstrophy dissipation as

$$\mathscr{K}(t) = \sum_{\boldsymbol{k}} k^2 N_k(t,t) \tag{5.4a}$$

$$\eta(t) = \sum_{\boldsymbol{k}} \hat{\nu}k^2 C_k(t,t). \tag{5.4b}$$

Following Frederiksen & Davies (2000) and Herring *et al.* (1974) we also define the large-scale Reynolds number $R_L(t)$ and the skewness $S_K(t)$ by

$$R_L(t) = \hat{\mathscr{E}}/\left(\hat{\nu}\eta^{1/3}\right) \tag{5.4c}$$

$$S_K(t) = 2\mathscr{K}/\left(\hat{\mathscr{P}}\hat{\mathscr{F}}^{1/2}\right), \tag{5.4d}$$

where, the transient energy, enstrophy, and palinstrophy are given by

$$\hat{\mathscr{E}}(t) = \tfrac{1}{2}\sum_{\boldsymbol{k}} C_{\boldsymbol{k}}(t,t)/k^2, \tag{5.4e}$$

$$\hat{\mathscr{F}}(t) = \tfrac{1}{2}\sum_{\boldsymbol{k}} C_{\boldsymbol{k}}(t,t), \tag{5.4f}$$

$$\hat{\mathscr{P}}(t) = \tfrac{1}{2}\sum_{\boldsymbol{k}} C_{\boldsymbol{k}}(t,t)k^2. \tag{5.4g}$$

The skewness S_K is a sensitive measure of the small-scale differences between the DNS and QDIA closure, while R_L provides a measure of the strength of the turbulence.

6. Numerical strategies

The numerical strategies that we use to solve the DNS and QDIA closure equations are very similar to those described by Frederiksen *et al.* (1994) and Frederiksen &

$\zeta(1,0)_4^1$	$\zeta(2,0)_4^2$	$\zeta(3,0)_4^3$	$\zeta(1,-2)_8^4$	$\zeta(1,-1)_4^5$	$\zeta(2,-2)_4^6$	$\zeta(k_x,k_y)_{degeneracy}^{label}$
$C_{(1,0)}$	$C_{(2,0)}$	$C_{(3,0)}$	$C_{(1,-2)}$	$C_{(1,-1)}$	$C_{(2,-2)}$	total
1.9634×10^{-7}	6.8372×10^{-7}	1.2664×10^{-6}	2.6716×10^{-4}	3.7414×10^{-7}	1.1677×10^{-6}	2.1523×10^{-3}
$\langle\zeta\rangle\langle\zeta^*\rangle_{(1,0)}$	$\langle\zeta\rangle\langle\zeta^*\rangle_{(2,0)}$	$\langle\zeta\rangle\langle\zeta^*\rangle_{(3,0)}$	$\langle\zeta\rangle\langle\zeta^*\rangle_{(1,-2)}$	$\langle\zeta\rangle\langle\zeta^*\rangle_{(1,-1)}$	$\langle\zeta\rangle\langle\zeta^*\rangle_{(2,-2)}$	total
1.1663×10^{-11}	4.5713×10^{-10}	8.9954×10^{-10}	5.4295×10^{-8}	1.0050×10^{-10}	7.8884×10^{-12}	2.6094×10^{-7}

TABLE 1. Initial conditions for C3 calculations.

Davies (2000). Both the DNS and closure equations use the predictor–corrector scheme for time-integration and the closure equations use the trapezoidal rule to evaluate the time-history integrals as originally employed by Kraichnan (1964*a*). For both the DNS and closure equations the interaction coefficients are precalculated as dense single-dimensional arrays and the fields, cumulants and response functions are calculated and stored for $\boldsymbol{k}$ in a half space, with complex conjugacy used to obtain the complete functions.

The DNS results are averages over large numbers of realizations in which the initial conditions are sampled from multivariate Gaussian distributions with specified mean and variance. Initial DNS sampling errors are reduced using strategies such as increasing the number of realizations in the ensemble and ensuring that for every perturbation from the mean in the ensemble there is also a perturbation with same structure but opposite sign. However, it should be noted that in time the nonlinearity in the evolution equation results in a sampling error arising in the determination of the DNS mean field. To illustrate this problem let us consider for example the simplest case of isotropic homogeneous turbulence. Then it can be readily shown that a non-zero mean field will evolve with time as the ensemble average in the DNS calculations even when there is no inhomogeneity in the dynamical equations. This is in contrast to the closure equations which maintain strict isotropy.

7. C3 resolution dynamics

In this section we examine the dynamics of the CUQDIA and QDIA closures and make comparison with DNS at resolution C3 for which $1\leqslant k\leqslant 3$. As Kells & Orszag (1978) noted, C3 has sufficient degrees of freedom to ensure that the systems are mixing. The closure calculations and DNS start from an initial state which is far from canonical equilibrium and for which the mean and transient (twice) enstrophy components are shown in table 1. The choice of very weak initial mean field components means that the evolved mean field is spun up as a direct result of the interaction of the transient eddies with the topography. In order to make close comparison with previous isotropic DIA C3 resolution calculations of Frederiksen *et al.* (1994) we start with isotropic initial conditions and use an isotropic topography with sprectrum given by (7.1). Thus, for the C3 resolution results (figure 1) the system has 28 components with degeneracy (the number of system components with the same transient enstrophy) given in table 1. The labels given to the components in table 1 are the same as shown in figure 1. The non-dimensional DNS and closure equations have been scaled by typical meteorological time and space scales; we use a length scale of half the earth's radius, 3.185610×10^6 m, and a time scale of $(\sqrt{2}\Omega)^{-1}$ with the earth's angular velocity $\Omega = 7.292\times10^{-5}\,\mathrm{s}^{-1}$. A single realization mean topography

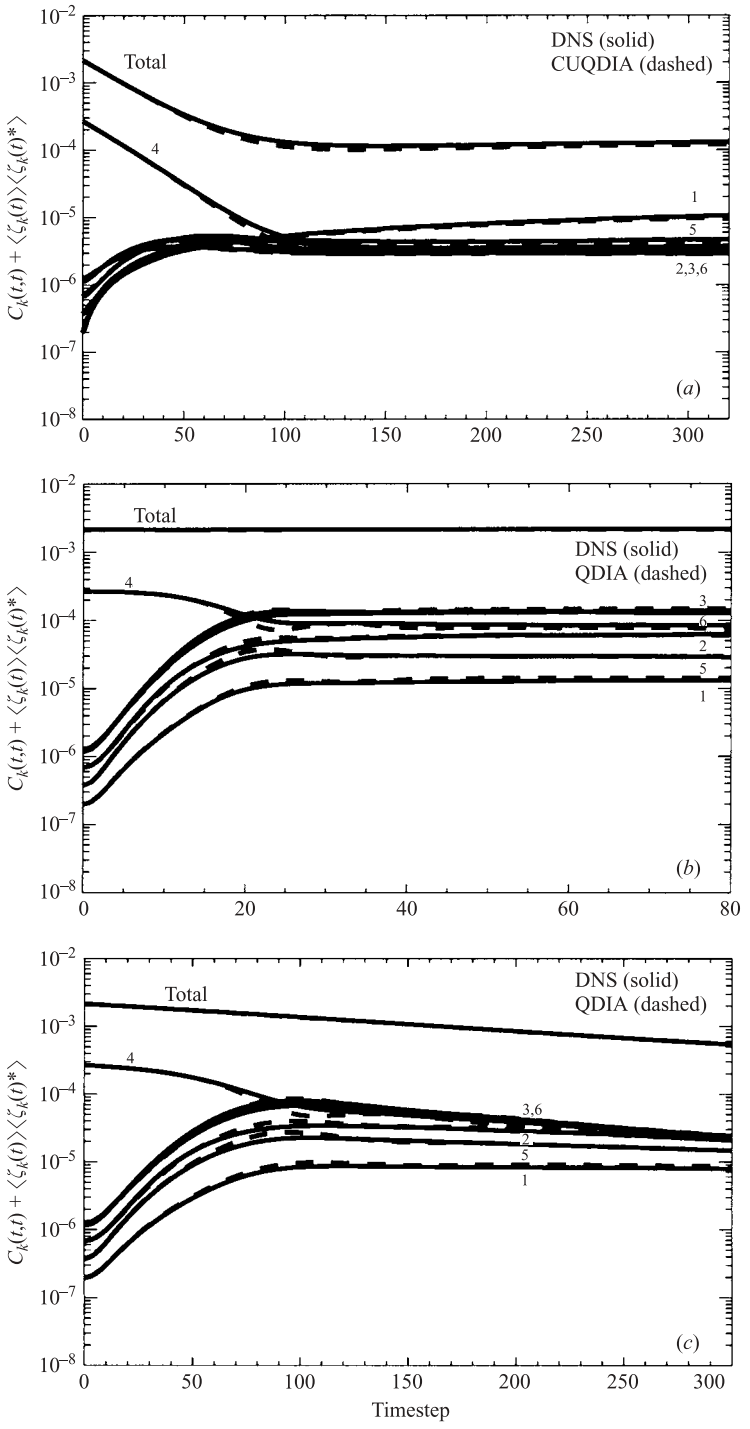

FIGURE 1. Comparison of DNS and closure results for the total fields in (*a*) (CUQDIA) the forced dissipative study, (*b*) (QDIA) the inviscid unforced case, and (*c*) (QDIA) for the dissipative case. Parameters are given in table 2.

Figure	Δt	$\hat{\nu}$	$\lvert h_{\boldsymbol{k}}\rvert^2$	$F^0_{\boldsymbol{k}}$	$\langle f^0_{\boldsymbol{k}}\rangle$	a	b
1(a)	2.2272	1.858×10^{-3}	$\dfrac{a+bk^2}{k^2b^2}$	$2\hat{\nu}k^2C^{eq}_{\boldsymbol{k}}$	$\hat{\nu}k^2\langle\zeta^{eq}_{\boldsymbol{k}}\rangle$	-5.969×10^5	7.444×10^5
1(b)	8.9088	0	$\dfrac{a+bk^2}{k^2b^2}$	0	0	-5.969×10^5	7.444×10^5
1(c)	2.2272	1.858×10^{-4}	$\dfrac{a+bk^2}{k^2b^2}$	0	0	-5.969×10^5	7.444×10^5

TABLE 2. Parameters for figure 1.

with amplitude squared

$$|h_{\boldsymbol{k}}|^2=(a+bk^2)/(k^2b^2) \tag{7.1}$$

is used. In this section all C3 DNS calculations represent an ensemble average over 5000 realizations with the initial real and imaginary parts of $\zeta_{\boldsymbol{k}}(0)$ having a joint Gaussian distribution. In the closure equations the cumulant update procedure starts with Gaussian initial conditions for which the off-diagonal terms are zero. The non-Gaussian and off-diagonal terms that build up with time are then used in the new initial conditions for subsequent restarts as detailed in § 3. The choice of parameters a and b (table 2) are comparable to those used by Frederiksen (1982) to study barotropic atmospheric flows.

7.1. *Forced-dissipative turbulent flow*

The first case we consider is for forced dissipative flow. The random forcing has variance determined by

$$F^0_{\boldsymbol{k}}=2\hat{\nu}k^2C^{eq}_{\boldsymbol{k}}, \tag{7.2a}$$

with the mean forcing specified by

$$\langle f^0_{\boldsymbol{k}}\rangle=\hat{\nu}k^2\langle\zeta^{eq}_{\boldsymbol{k}}\rangle=-\tfrac{1}{2}bh_{\boldsymbol{k}}F^0_{\boldsymbol{k}}. \tag{7.2b}$$

Here the canonical equilibrium values for the transient enstrophy and mean vorticity components are determined by

$$C^{eq}_{\boldsymbol{k}}=k^2/(a+bk^2) \tag{7.2c}$$

$$\langle\zeta^{eq}_{\boldsymbol{k}}\rangle=-bh_{\boldsymbol{k}}C^{eq}_{\boldsymbol{k}} \tag{7.2d}$$

and this ensures that the system is forced to evolve towards canonical equilibrium. The choice of topographic strength, (7.1), in combination with the specified forcing, (7.2), ensures that the system evolves from an initial disequilibrium state (table 1) that is dominated by transients to a canonical equilibrium state in which the mean and transient enstrophy component amplitudes are equal.

In figure 1(a) we show the dynamical evolution over an 80-day integration for the total enstrophy components with cumulant updates at every 5 days. The timestep used is 1/4 day where 1 day has a non-dimensional value equal to 8.9088. The numerical parameters are detailed in table 2. Close agreement between the closure and DNS results is shown at all time periods as the system evolves from an initial disequilibrium state toward canonical equilibrium under the effects of forcing and dissipation. A comparison of the QDIA and CUQDIA results (not shown) indicates close agreement (6 significant figures in the total enstrophy components). We also note that an ensemble average of 5000 realizations in the DNS calculation cannot ensure

exact isotropy in the 28 components of the C3 truncation resulting in a maximum relative error in the enstrophy components of approx. 3% spread in simulations (Frederiksen *et al.* 1994). The closures perform very well when both forcing and dissipation are present. However, a more stringent test is to consider the performance of the QDIA closure for inviscid unforced or viscous decaying flows. These cases are discussed in the following subsection.

7.2. *Inviscid unforced flow and viscous decaying turbulent flow*

Figures 1(*b*) and 1(*c*) present analogous results to those in figure 1(*a*) but for inviscid unforced flow and viscous decaying flow, respectively. These calculations are again started with the same initial disequilibrium state as that used in the forced dissipative calculation and are evolved over similar time periods. Details of the parameters used are included in table 2. For both cases we use the QDIA closure without cumulant updates. The closure clearly captures the initial growth and decay phase of the total enstrophy components. This initial period out to day 20 is also when the mean field is being generated. The moderate amplitude oscillations evident in the closure between days 20 and 40 are very similar to those reported by Frederiksen *et al.* (1994) in their study of closure theories for severely truncated two-dimensional isotropic turbulence. These oscillations result in the QDIA closure very slightly underpredicting the crossover time for the decaying enstrophy component (1,−2) and the two fastest growing enstrophy components (3,0) and (2,−2). In general it is found that the QDIA oscillations are somewhat reduced in amplitude relative to those present in the DIA due to the presence of topography and mean-field. Since such oscillations are a feature of the DIA it is reasonable to assume that they arise from inaccuracies in the treatment of the triple cumulant term. The viscous decay calculation in figure 1(*c*), was run with a timestep of 1/4 days in order to ensure stability over a 75-day time period. The viscous decay run displayed similarly close agreement with DNS to that seen in the inviscid unforced experiment (figure 1*b*) where a timestep of 1 day was used over an 80-day period. Both cases are in close agreement with DNS in the early (0–15 days) and later (+40 days) periods with slight difference only due to the oscillatory phase in the closure occurring between days 15 and 40.

8. Very low Reynolds number turbulence

Next, we consider two cases of the viscous decay of flows at very low Reynolds number ($R_L(0) \approxeq 0.02$) and for resolutions C48 and C64. The purpose of these experiments is to ascertain the validity of the quasi-diagonal closure approach for the incorporation of topography and mean-field in a setting devoid of the effects of strong turbulence. These studies will underpin our later investigations as we progressively incorporate the effects of stronger turbulence for a variety of topographies. The two cases considered in this section have the same topographic and transient fields but with different mean fields and resolutions. The form of the topographic amplitude considered in this section is given by (7.1) with random phase as in (2.5). All parameters for cases I and II are specified in table 3. Throughout this section the restart time is $T = 10$ for the cumulant update closure.

8.1. *Case I*

In figure 2(*a–d*) we show the results for viscous decay calculations at C48 resolution with DNS and CUQDIA closure in which the initial disequilibrium field is constructed by using (7.2*c*) and setting $\langle \zeta_{\boldsymbol{k}}(0) \rangle = -1/10 \times b h_{\boldsymbol{k}} (k^2/(a + bk^2))$. The system is evolved to a final time $t_f = 0.4$. The initial mean kinetic energy field (figure 2*a*) is $\approx$ 2 orders

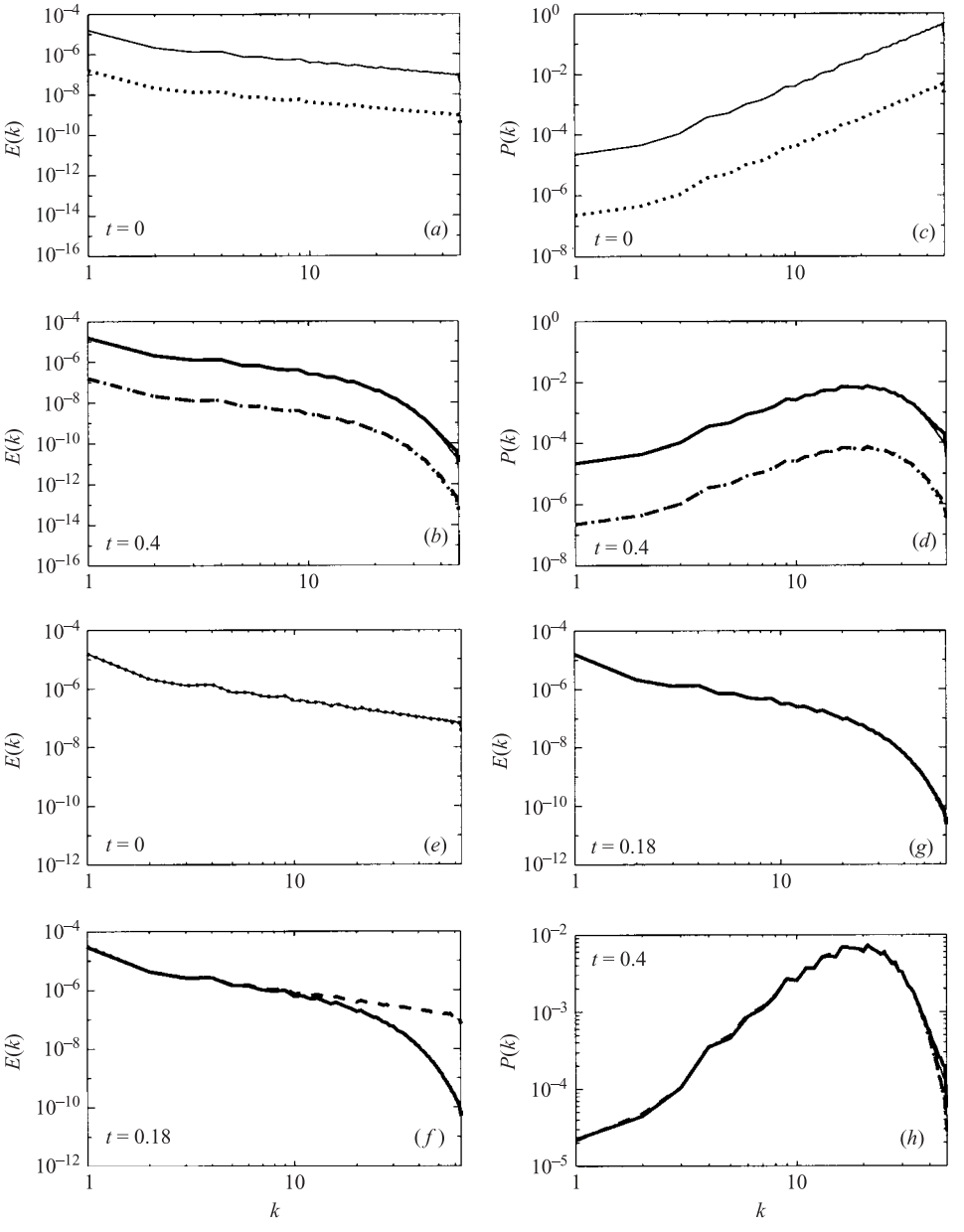

FIGURE 2. Case I. Comparison of CUQDIA and DNS at C48 resolution for viscous decay at very low Reynolds number. Throughout the evolved CUQDIA and DNS spectra are only distinguishable at the smallest scales. Kinetic energy (left column); Palinstrophy (right column). (a,c) Initial mean and transient fields. (b,d) Mean and transient fields at $t=0.4$. Component field diagrams: mean field; DNS (dashed), CUQDIA (dotted): transient field; DNS (thick solid), CUQDIA (thin solid). Case II. Viscous decay from an initial equilibrium state at C64 resolution. (e) Initial mean and transient kinetic energy. (g) Mean and transient kinetic energy at $t=0.18$. (h) The same calculation run out to $t=0.4$ now for C48 resolution where we consider the component fields of the palinstrophy. In diagrams $(e,g$ and $h)$ the component field diagrams are labelled as for (a)–(d). (f) Total kinetic energy: initial (dashed), DNS (solid), CUQDIA (dotted).

Figure	Δt	$\hat{\nu}$	$C_{\boldsymbol{k}}(0,0)$	$\lvert h_{\boldsymbol{k}}\rvert^2$	$\langle\zeta_{\boldsymbol{k}}(0)\rangle$	a	b
2(a–d)	0.004	0.005	$C_{\boldsymbol{k}}^{eq}$	$\dfrac{a+bk^2}{b^2k^2}$	$0.1\times\langle\zeta_{\boldsymbol{k}}^{eq}\rangle$	-5.969×10^5	7.444×10^5
2(e–h)	0.004	0.005	$C_{\boldsymbol{k}}^{eq}$	$\dfrac{a+bk^2}{b^2k^2}$	$\langle\zeta_{\boldsymbol{k}}^{eq}\rangle$	-5.969×10^5	7.444×10^5

TABLE 3. Parameters for figure 2.

of magnitude weaker than the initial transient energy. Thus it is interesting to note that as the total energy decays the mean and transient fields decay at approximately the same rate (figure 2b). This is also seen in the diagrams depicting the evolution of the palinstrophy fields (figures 2c and 2d). Throughout, the CUQDIA is in such close agreement with DNS as to be indistinguishable apart from some very slight difference between the transient fields at the very smallest scales.

8.2. *Case II*

The experiments with DNS and CUQDIA closure displayed in figure 2(e–h) correspond to viscous decay from an initial canonical equilibrium state. The choice of topographic amplitude and parameters (table 3) gives initial mean and transient fields of equal magnitude. The system is now evolved to $t_f = 0.18$ at C64 resolution. As previously in figure 2(a–d), we again see the component fields decaying at the same rate (figure 2e, g and h). The initial and final large-scale Reynolds numbers are again < 1. We note that the evolved C64 DNS and CUQDIA closure results in figure 2 are virtually indistinguishable. In figure 2(h) the same calculation is performed at C48 resolution to a final time $t_f = 0.4$ where we again have very close agreement between all DNS and CUQDIA spectra but for some very slight under-representation of the CUQDIA transients for $40 < k < 48$. A further case of viscous decay from canonical equilibrium with a weak small-scale topographic amplitude $|h_{\boldsymbol{k}}|^2 = 16k^2/(1+k^3)^2$ (not shown) with similar large-scale Reynolds numbers was also studied at C64 resolution; again very close agreement between DNS and CUQDIA spectra was found for evolved times out to $t_f = 0.18$.

9. Low Reynolds number turbulence

In the experiments of the previous section the Reynolds number was purposely kept very low (< 1) in order to test the quasi-diagonal closure performance in the absence of strong turbulence effects. In this section we will consider low Reynolds number turbulence ($R_L \approx 60$) making direct comparisons with the previous isotropic turbulence studies of Herring *et al.* (1974) and Frederiksen & Davies (2000). Our initial transient enstrophy spectrum corresponds exactly to spectrum A of Frederiksen & Davies (2000) and closely to spectrum I of Herring *et al.* (1974). The initial transient spectrum A (9.1a) is coupled to an initial mean vorticity field (9.1b):

$$\text{(Spectrum A)} \qquad C_{\boldsymbol{k}}(0,0) = 1.33\times10^{-4}k^5\exp(-k^2/32), \tag{9.1a}$$

$$\langle\zeta_{\boldsymbol{k}}(0)\rangle = -bh_{\boldsymbol{k}}\frac{k^2}{a+bk^2}. \tag{9.1b}$$

We consider two cases with topographic amplitudes whose squared values are $16k^2/(1+k^3)^2$ (case AI) and $4/(1+k)^2$ (case AII) respectively. In the first case the

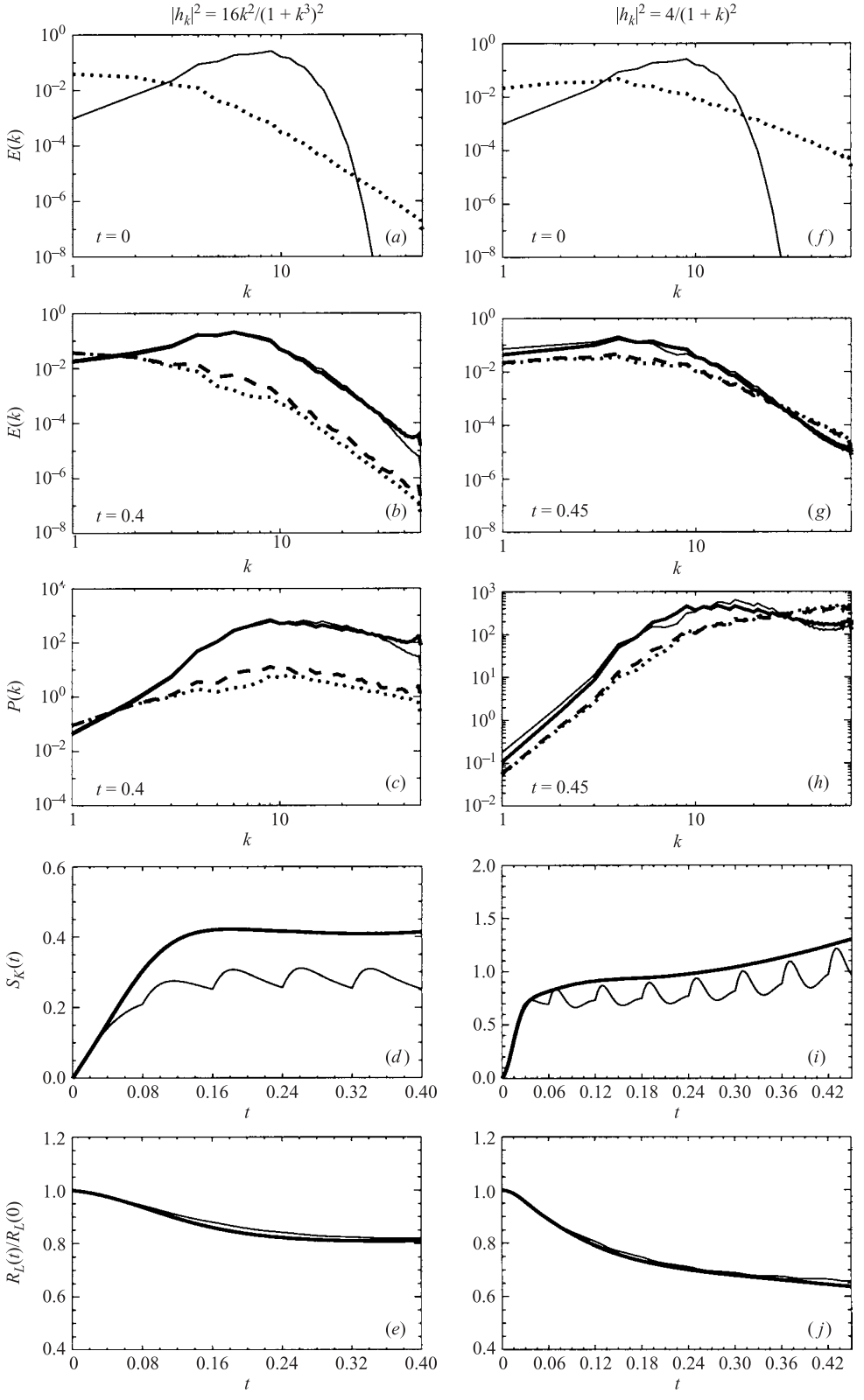

FIGURE 3. For caption see facing page.

topography falls away as $h_{\boldsymbol{k}} \approx 1/k^2$ while in the second case it scales as $h_{\boldsymbol{k}} \approx 1/k$. These two cases represent significantly different small-scale topographic strengths and initial mean fields. The parameters used are given in table 4. Cumulant updates are at every 20 timesteps for the CUQDIA calculations in both cases. The DNS spectra represent an ensemble average of 100 realizations with standard deviations (not shown) comparable to those in figures 1, 3 and 4 of Frederiksen & Davies (2000). The calculations start from Gaussian initial conditions for which the off-diagonal elements of the two-point cumulants are zero. We use a non-dimensional viscosity of $\hat{\nu} = 0.005$ which gives an initial Reynolds number of $R_L \approxeq 62$ for both DNS and the closure. We compare the DNS and CUQDIA performance using the evolved kinetic energy, palinstrophy, skewness and large-scale Reynolds number as diagnostics. The choice of parameters a and b (table 4) are the same as Frederiksen & Sawford (1980) used to fit the large scales of meteorological flows.

9.1. *Case AI*

We consider first case AI at C48 resolution for which the topography scales like $1/k^2$. The mean and transient kinetic energy spectra for the initial conditions are shown in figure 3(a). In figures 3(b) and 3(c) we compare the DNS and CUQDIA evolved energy and palinstrophy spectra at $t = 0.4$, corresponding to 100 timesteps with a non-dimensional timestep $\Delta t = 0.004$. Although only half the time period considered in the earlier isotropic studies of Frederiksen & Davies (2000) and Herring *et al.* (1974), the system has undergone very significant evolution. The rapid development of the flow fields can be attributed to the presence of both the topography and mean-field.

A comparison of figures 3(b) and 3(c) with figure 1 of Frederiksen & Davies (2000) and figures 18 and 19 of Herring *et al.* (1974) reveals a much more dramatic and rapid increase in the total energy and palinstrophy at the smallest scales when topography and a mean-field are present. In the early stages of the evolution this would seem to be due to the relatively large amplitude $\langle \zeta_{\boldsymbol{k}}(t) \rangle$ and $h_{\boldsymbol{k}}$ forcing the tendency of the transients at the small scales rather rapidly via the $P_{\boldsymbol{k}}$ and $\pi_{\boldsymbol{k}}$ terms in the cumulant equation ((3.5) and (3.6)). However, in the later stages when the transients dominate at all scales, it is primarily the transfer of energy from the intermediate-scale transients that causes the subsequent growth in the small-scale transients in a similar manner to the behaviour found in the isotropic studies of Frederiksen & Davies (2000). In figures 3(b) and 3(c) the transient energy and palinstrophy spectra have undergone rapid increase at the small scales, whereas the mean energy and palinstrophy fields have evolved much less significantly. We see very close agreement between the CUQDIA and DNS transient fields except at the very smallest scales.

In figures 3(d) and 3(e) the DNS and CUQDIA skewness and large-scale Reynolds number are compared. In figure 2(c) of Frederiksen & Davies (2000) it was shown that the discrete closure resulted in a very much improved estimation of the skewness

---

FIGURE 3. Low Reynolds number spectra. The left column results are for case AI at C48 resolution and the right column results are for case AII at C64 resolution. (a, f) Initial mean and transient energy spectra. (b, g) Evolved mean and transient energy fields. (c, h) Mean and transient palinstrophy spectra at $t = 0.4$ and $t = 0.45$ respectively. Component field diagrams: mean field; DNS (dashed), CUQDIA (dotted): transient field; DNS (solid), CUQDIA (thin solid). (d, i) Skewness and (e, j) $R_L(t)/R_L(0)$ evaluated at time t. DNS (solid) and CUQDIA (thin solid), with restarts calculated at every 20 timesteps. Parameters are given in table 1.

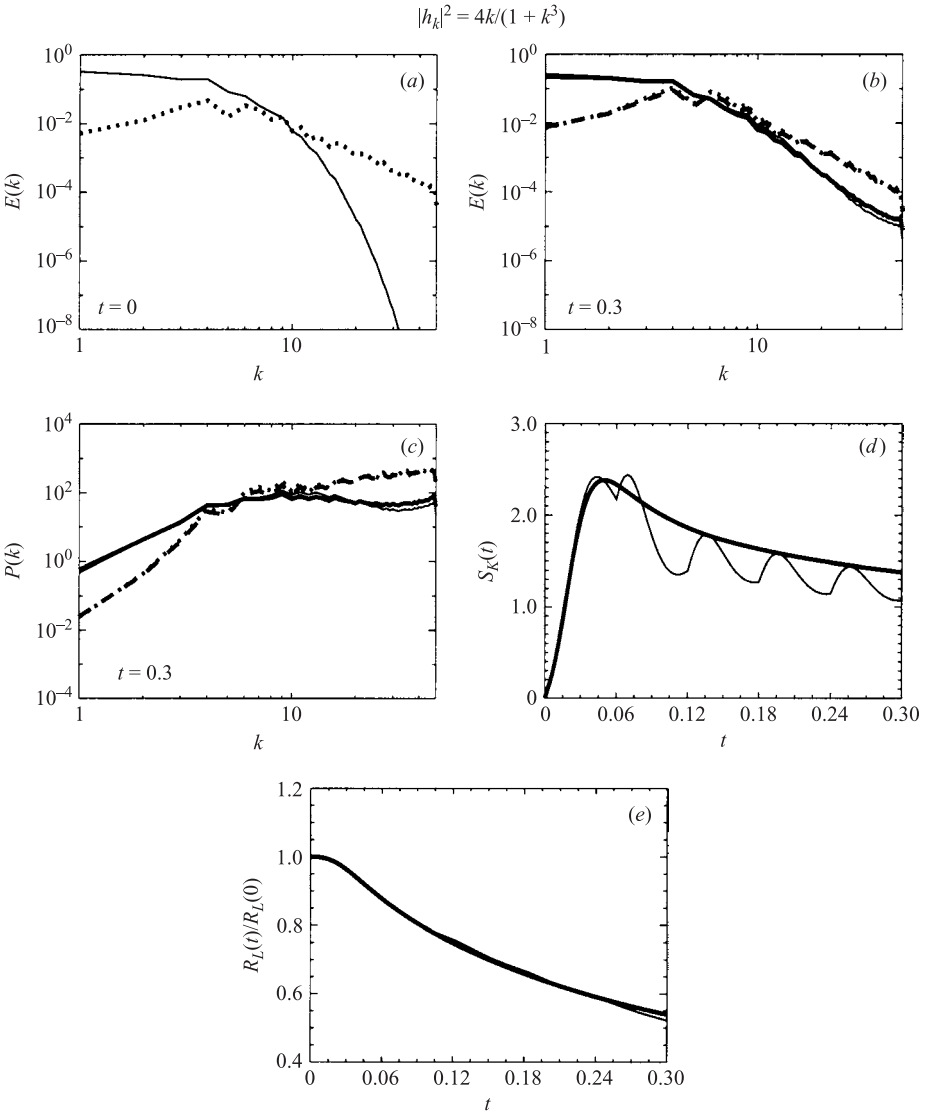

FIGURE 4. Case BI, C48 resolution spectra. The initial mean and transient energy spectra are depicted in (*a*) with the final evolved energy and palinstrophy fields shown in (*b*) and (*c*), respectively. The component field diagrams are as follows: DNS mean-field (dashed), CUQDIA mean-field (dotted), DNS transient-field (thick solid), CUQDIA transient-field (thin solid). The skewness (*d*) and the large-scale Reynolds number (*e*) for DNS (thick solid) and CUQDIA (thin solid).

in comparison to the continuous DIA closure (Herring *et al.* 1974*a*, figure 12). For inhomogeneous flow over topography we see that the CUQDIA spectra have rapidly evolved to much larger small-scale amplitude than for similar isotropic studies. The final values are $S_K^{CUQDIA}(0.4) = 0.25$ as compared to $S_K^{DNS}(0.4) = 0.41$. This result gives an indication of the importance of the additional eddy-mean field and eddy-topographic interactions not present in previous isotropic studies. A comparison of the large-scale Reynolds number for DNS and the closure (figure 3*e*) reveals good agreement throughout the evolution to $t_f = 0.4$.

Figure	Δt	$\hat{\nu}$	$\lvert h_{\boldsymbol{k}}\rvert^2$	a	b
3(a–e)	0.004	0.005	$16k^2/(1+k^3)^2$	4.824×10^4	2.511×10^3
3(f–j)	0.003	0.005	$4/(1+k^2)$	4.824×10^4	2.511×10^3
4(a–e)	0.003	0.0025	$4k/(1+k^3)$	4.824×10^4	2.511×10^3

TABLE 4. Parameters for figures 3 and 4.

9.2. *Case AII*

For case AII, we use a C64 resolution and a topography which scales like $1/k$ resulting in a larger amplitude small-scale mean field. The mean and transient kinetic energy spectra for the initial conditions are shown in figure 3(f). The evolved kinetic energy (figure 3g) and palinstrophy (figure 3h) spectra show that the mean field still dominates the small scales at $t_f = 0.45$ (150 timesteps with $\Delta t = 0.003$). We note that there is close agreement between DNS and CUQDIA at all scales apart from slight differences at the very largest scales with $k = 1$ and 2.

The CUQDIA skewness in figure 3(i) depicts the typical cycle of growth and decay following each update time discussed by Frederiksen & Davies (2000). The CUQDIA skewness again underestimates the DNS skewness ($S_K^{CUQDIA}(0.45) = 0.98$, $S_K^{DNS}(0.45) = 1.30$) but less so than for case AI with the weaker small-scale topography. Again, the large-scale Reynolds number for the CUQDIA closure (figure 3j) closely matches the DNS results.

10. Moderate Reynolds number turbulence

Next we consider moderate Reynolds number turbulence and compare the performance of the regularized CUQDIA (RCUQDIA) closure with DNS and the CUQDIA closure. A range of cases with qualitatively different initial spectra are examined. For cases BI and BIII the simulations and closure calculations start from an initial transient spectrum, denoted spectrum B, which is specified by:

$$\text{(Spectrum B)} \quad C_{\boldsymbol{k}}(0,0) = 1.8\times10^{-1}k^2\exp\left(-\tfrac{2}{3}k\right). \tag{10.1a}$$

This spectrum is identical to Spectrum B of Frederiksen & Davies (2000) and is also very similar to spectrum II of Herring *et al.* (1974) and has an initial large-scale Reynolds number of $\approx$305. In case BI the initial mean contribution is determined by

$$\langle\zeta_{\boldsymbol{k}}(0)\rangle = -bh_{\boldsymbol{k}}\frac{k^2}{a+bk^2}, \tag{10.1b}$$

with topographic amplitude squared of $\lvert h_{\boldsymbol{k}}\rvert^2 = 4k/(1+k^3)$ (case BI). In case BI parameters a and b are again as in §9 (see table 4). In cases BII and BIII the topography has the form $\lvert h_{\boldsymbol{k}}\rvert^2 = 1.8\times10^{-3}\exp(-\frac{2}{3}k)$ while the initial mean fields are not determined by an analytic form but are as shown in figures 5 and 6. For case BII the initial transient spectrum is also not given by (10.1a) but is as shown in figure 5(a). In all cases the phase of the topography is fixed but random as in (2.5). Throughout this section the restart time is $T = 20$ for the cumulant update closures.

10.1. *Case BI*

The first study (case BI) we consider has the same initial transient kinetic energy specified through Spectrum B. The topography ($\lvert h_{\boldsymbol{k}}\rvert^2 = 4k/(1+k^3)$) and mean field (10.1$b$) are dominant at the small scales while the transients dominate the large

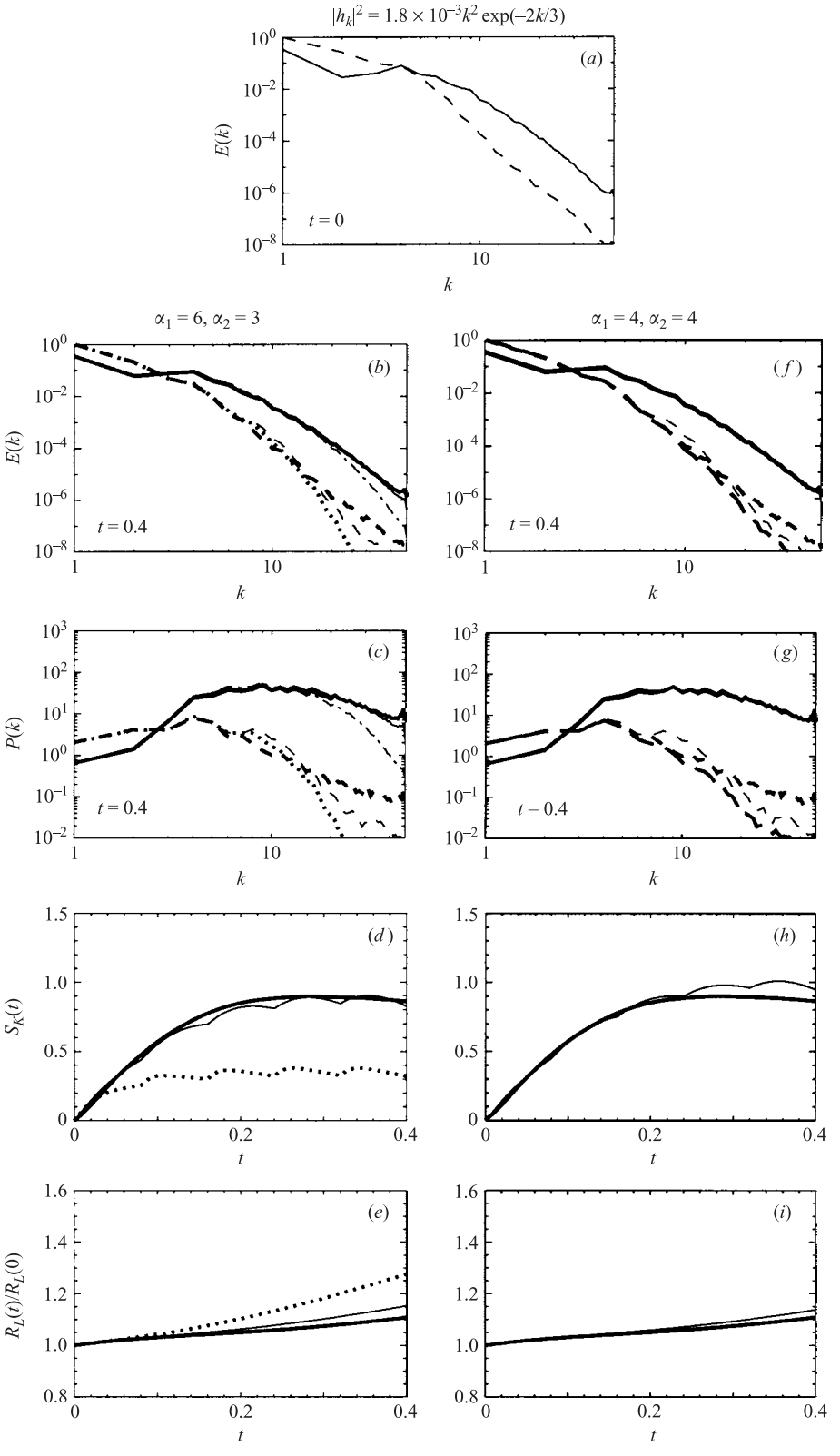

FIGURE 5. For caption see facing page.

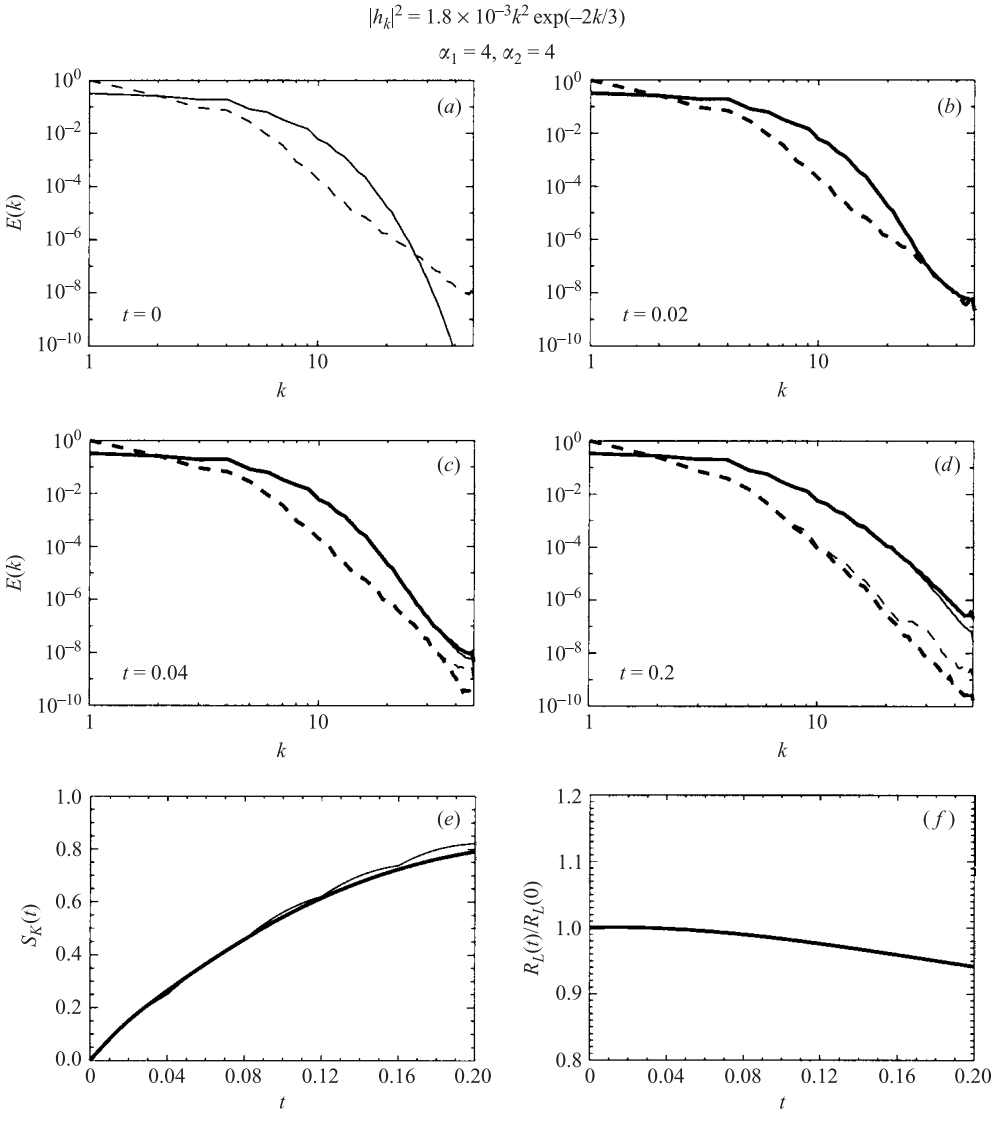

FIGURE 6. Case BIII. Comparison of DNS and RCUQDIA at C48 resolution for $R_L = 304.84$. (*a*) Initial mean (thin dashed) and transient (thin solid) kinetic energy. (*b–d*) Mean and transient kinetic energy spectra at $t = 0.02$, 0.04 and 0.2, respectively. Component field diagrams: mean field; DNS (1000 member ensemble, thick dashed), RCUQDIA (thin dashed): transient field; DNS (1000 member ensemble, thick solid), RCUQDIA (thin solid). (*d*) Skewness and (*e*) $R_L(t)/R_L(0)$. DNS (thick solid) and RCUQDIA (thin solid) with restarts calculated at every 20 timesteps.

FIGURE 5. Case BII. Comparison of DNS with CUQDIA and RCUQDIA closures at C48 resolution. Parameters can be found in table 5. (*a*) Initial mean (thin dashed) and transient (thin solid) kinetic energy. (*b*, *f*) Mean and transient kinetic energy spectra at $t_f = 0.4$. (*c*, *g*) Mean and transient palinstrophy spectra at $t_f = 0.4$; Component field diagrams: mean field; DNS (100 member ensemble, thick dashed: 1000 member ensemble, thick long dashed), CUQDIA (thick dotted), RCUQDIA (thin dashed): transient field; DNS (100 member ensemble, thick solid: 1000 member, thin long dashed), CUQDIA (thin dot dashed), RCUQDIA (thin solid). (*d*, *h*) Skewness and (*e*, *i*) $R_L(t)/R_L(0)$ evaluated at time t. DNS (thick solid), CUQDIA (thick dotted) and RCUQDIA (thin solid) with restarts calculated at every 20 timesteps.

Figure	Δt^{CUQDIA}	Δt^{DNS}	$\hat{\nu}$	$\lvert h_{\boldsymbol{k}}\rvert^2$
5	0.004	0.002	0.002	$1.8\times10^{-3}k^2\exp\left(-\frac{2}{3}k\right)$
6	0.002	0.002	0.0025	$1.8\times10^{-3}k^2\exp\left(-\frac{2}{3}k\right)$

TABLE 5. Parameters for figures 5 and 6.

scales. In figure 4(a) the initial mean and transient spectra are displayed. At the nondimensional time of $t_f = 0.3$ the evolved CUQDIA mean and transient kinetic energy spectra (figure 4b) are shown to be in close agreement with DNS apart for some slight underestimation of the closure transient field at the small scales. The mean and transient palinstrophy spectra (figure 4c) show similar agreement between DNS (100 realizations) and the closure transient fields, and highlight the very close agreement in the respective mean fields. In figure 4(d) it is evident that the closure skewness underestimates that of the DNS, but that the differences are considerably less than without topography present as seen in comparison with figure 3 of Frederiksen & Davies (2000). The final evolved values are $S_K^{DNS}(0.3) = 1.379$ and $S_K^{CUQDIA}(0.3) = 1.070$, respectively. The Reynolds number in the closure evolves very similarly to that of the DNS (figure 4e) with the final evolved values of $R_L^{DNS}(0.3) = 164$ and $R_L^{CUQDIA}(0.3) = 159$. It is of note that for cases where the small-scale topography is strong the closure and DNS evolved energy, palinstrophy and Reynolds number agree very closely with DNS despite the closure underestimating the skewness by up to 25%.

10.2. *Case BII*

For case BII, the conditions from which the simulations and closure calculations are started are not given by an analytic form but the initial mean and transient kinetic spectra are as shown in figure 5(a). Case BII has mean and transient kinetic energy spectra which have broad similarities with typical atmospheric spectra (Boer & Shepherd 1983). In particular, at large scales the mean flow dominates while at intermediate and small scales the transients dominate the kinetic energy spectrum. This situation continues as the flow evolves. These properties are in part related to the choice of topography (table 5) that ensures strong mean-field topographic interactions at large scales but negligible coupling at the smallest scales allowing the eddy–eddy interactions to dominate there. For this initial state the large-scale Reynolds number is $R_L \approxeq 202$.

We have experimented with the choice of regularization parameters α_1 and α_2 in the RCUQDIA closure but will focus on results for $\alpha_1 = 6$, $\alpha_2 = 3$ (figure 5b–e) and $\alpha_1 = \alpha_2 = 4$ (figure 5f–i). The choice $\alpha_1 = 6$, $\alpha_2 = 3$ was made to make direct comparison with the regularized DIA (RDIA) studies of Frederiksen & Davies (2003). They found that the performance of the RDIA and RCUDIA closures for isotropic turbulence without a mean field was close to optimal with $\alpha_1 = 6$ and for a variety of spectra with large-scale Reynolds numbers up to $\approx$4000. The choice of $\alpha_2 = 3$ was then made on the basis of experimentation. This also suggested that a one-parameter closure, with say $\alpha_1 = \alpha_2 = 4$, might perform as well for a wide variety of flows provided the mean and transient fields were of comparable magnitudes.

In figure 5 we compare the performance of the RCUQDIA closure for $\alpha_1 = 6$, $\alpha_2 = 3$ and $\alpha_1 = \alpha_2 = 4$ with the results of DNS and CUQDIA closure calculations. The statistics are evolved to $t_f = 0.4$ and the timesteps used for the closures and DNS, as well as the viscosity in these viscous decay calculations, are given in table 5. For the DNS we compare results for 100 and 1000 member ensembles in order to examine the sampling problem of determining the mean field and variance which was discussed in § 6. Figures 5(*b*) and 5(*f*) compare the evolved kinetic energy spectra and figures 5(*c*) and 5(*g*) the evolved palinstrophy spectra for the two DNS calculations, the two RCUQDIA calculations and the CUQDIA results. We note that the CUQDIA mean and transient spectra have too small amplitudes compared with DNS at the smaller scales. In contrast, the RCUQDIA transient spectra, for both choices of cutoff parameters, compare closely with the DNS ensemble averages for both the 100 and 1000 member ensembles. In particular, the transient spectra for the RCUQDIA for both pairs of cutoff ratios are nearly indistinguishable from the DNS results. The RCUQDIA mean field also compares most closely to the 1000 member ensemble DNS results at small scales, although there does appear to be a slight over-estimation of the RCUQDIA mean field for the small scales. The differences in the two DNS are due to the sampling problem with the DNS spectra flattening out at small scales (figures 5*f* and 5*g*) where the mean field in the 100 member DNS ensemble approaches the 1 percent sampling error barrier. In contrast, the 1000 member ensemble is better able to resolve the mean field at small scales.

Figures 5(*d*) and 5(*h*) show the evolution of the skewness for the closures and DNS. We note that the RCUQDIA skewness, for both pairs of cutoff parameters, is in excellent agreement with the DNS skewness. In contrast the CUQDIA skewness is significantly less than for the DNS; at $t_f = 0.4$ we find that $S_K^{DNS} = 0.86$, $S_{K_{\alpha_1=6,\alpha_2=3}}^{RCUQDIA} = 0.83$, $S_{K_{\alpha_1=4,\alpha_2=4}}^{RCUQDIA} = 0.95$ while $S_K^{CUQDIA} = 0.32$. Again, figures 5(*e*) and 5(*f*) show that the regularized closures accurately predict the evolution of the DNS Reynolds number, while the CUQDIA closure slightly overestimates the evolved Reynolds number. At $t_f = 0.4$ $R_L^{DNS} \approx 223$, $R_{L_{\alpha_1=6,\alpha_2=3}}^{RCUQDIA} \approx 233$, $R_{L_{\alpha_1=4,\alpha_2=4}}^{RCUQDIA} \approx 229$, while $R_L^{CUQDIA} \approx 257$.

10.3. *Case BIII*

We now consider case BIII where $C_k(0, 0)$ is given by spectrum B and the initial mean field and topography are as for the previous case, case BII. This set of initial conditions again corresponds to an initial large scale Reynolds number of ≈ 305 with the mean field dominating the very largest and very smallest scales. This choice of initial conditions results in very rapid and complex evolution in both the small scale transients and mean fields. For this case we have chosen to study the accuracy of the closure in capturing this early period of rapid development. As for case BII, in comparison to DNS optimal results were found for $\alpha_1 = \alpha_2 = 4$. The DNS results are an average of 1000 realizations. In figure 6(*a*)–(*d*) we clearly observe the rapid transfer of energy to the small-scale transients in the period to $t = 0.02$ with little loss from the small scales of the mean field. The subsequent evolution of the energy spectra shows continuing transfer from the small scales of the mean field as the small-scale transients grow. Throughout, the closure compares closely to DNS. In figures 6(*e*) and 6(*f*) the closeness of the results are clear in the evolved skewness with $S_{K_{\alpha_1=4,\alpha_2=4}}^{RCUQDIA} = 0.82$ comparing well to $S_K^{DNS} = 0.79$. Similarly the final evolved $R_{L_{\alpha_1=4,\alpha_2=4}}^{RCUQDIA} = 287.5$ is very close to the DNS value $R_L^{DNS} = 287.0$.

10.4. *Additional results*

In addition to the cases discussed above a large number of numerical experiments were conducted in order that a significant portion of parameter space be examined. Of particular note a case intermediate between case BI and cases BII and BIII was also studied. For this intermediate case the initial transient spectrum was again spectrum B; however the mean contribution was determined by (10.1*b*) with a topography for which $|h_{\boldsymbol{k}}|^2 = 16k^2/(1+k^3)^2$ and with all other parameters the same as for case BI (see table 4). The QDIA closure without regularization was again found to underestimate the evolved skewness and small-scale kinetic energy, while for the regularized QDIA close agreement to DNS was once again found for $\alpha_1 = \alpha_2 = 4$. Importantly $\alpha_1 = \alpha_2 = 4$ was found to be almost universal over a large range of experiments for cases with moderate Reynolds number and weak small-scale topography.

11. Discussion and conclusion

The performance of the QDIA closure for inhomogeneous turbulence over topography has been examined and compared with the statistics of DNS for resolutions $1 \leqslant k \leqslant k_{max}$ with k_{max} ranging from 3 (C3) to 64 (C64), and for a range of Reynolds numbers between very low ($R_L < 1$) and moderate ($R_L \approx 300$). Studies have been performed for a wide range of initial conditions and topographies. We have also formulated cumulant update closures, in which the time-history integrals in the QDIA closure are periodically truncated and the off-diagonal two-point cumulant and the three-point cumulant are used in the initial conditions of the restart procedure. The cumulant update closure QDIA (CUQDIA) is much more efficient making long-time integrations possible, and has similar performance to the QDIA closure provided the restart or update time T is not too short. At moderate Reynolds number ($R_L \approx 300$) we have also examined a regularized version of the CUQDIA closure (RCUQDIA). The regularization localizes eddy–eddy, eddy-mean field and eddy-topographic interactions between the large-scale and small-scale eddies depending on specified cut-off ratios α_1 and α_2. The RCUQDIA closure almost universally compared most closely with DNS for $\alpha_1 = \alpha_2 = 4$, thus producing a one-parameter inhomogeneous non-Markovian theory for flow over topography. The RQDIA (resp. RDIA) is a one-parameter two-time non-Markovian closure for inhomogeneous (resp. homogeneous) turbulence just as the popular TFM (Kraichnan 1971*a*, *b*), EDQNM (Orszag 1970, 1973, Leith 1971) and RTFM (Bowman & Krommes, 1997) are one-parameter single-time Markovian closures for homogeneous turbulence. Regularization corresponds to a simple empirical form of vertex renormalization which localizes transfers and ensures that the decay time of the two-time cumulant and response functions at high wavenumber are determined by local excitation levels (Kraichnan 1964*c*; Frederiksen & Davies 2003). As a consequence the inability of the Eulerian DIA to distinguish accurately between convection and distortion effects of small-scale eddies by large-scale eddies is corrected resulting in improved small-scale spectra.

We have found that the dynamics and spectra of QDIA and CUQDIA closures agree very closely with the statistics of DNS at very low Reynolds number and for resolutions ranging from C3 to C64. In particular, the time evolution of enstrophy components at C3 resolution has demonstrated that the QDIA and CUQDIA are in close agreement and also more closely match DNS results in the early period of growth and oscillatory behaviour of the modes than found in related isotropic DIA calculations (see Frederiksen *et al.* 1994). These results have been established in forced-dissipative, viscous decay and inviscid unforced calculations. Further viscous

decay experiments at higher C48 and C64 resolutions and at very low Reynolds numbers have established close agreement between closures and DNS. Thus, when turbulence is weak, the quasi-diagonal approximation (Frederiksen 1999) for the incorporation of topography and mean-field in closure models performs extremely well.

Our low Reynolds number runs ($R_L \approx 60$) have examined the viscous decay of turbulence in two cases with the same transient spectra but with different small-scale topographic amplitudes and initial mean fields. In the first case, case AI, the topography scales like $1/k^2$ while in the second, case AII, it falls off more slowly like $1/k$ and the mean fields have corresponding behaviour.

For case AI, at resolution C48, the evolved kinetic energy and palinstrophy spectra for the CUQDIA closure are found to compare closely with DNS results except for a slight overestimation at the smallest scales ($k \geqslant 35$) despite the CUQDIA closure underpredicting the evolved skewness. The evolution of the transient small-scale spectra is much more rapid when topography and a mean field are present than in corresponding isotropic turbulence calculations of Frederiksen & Davies (2000) and Herring *et al.* (1974). This appears to be due to the topography and mean field rapidly forcing the tendency of the small-scale transients in the early stages of evolution.

For case AII, at resolution C64, the mean field still dominates the kinetic energy and palinstrophy spectra at small scales at the end of the time period of interest ($t_f = 0.45$). In this case there is close agreement between CUQDIA and DNS spectra at most scales. Here the agreement between the CUQDIA and DNS also extends more closely to the skewness which is a very sensitive measure of small scale differences. For both cases AI and AII the evolution of the large-scale Reynolds number for the closure closely follows that of the DNS.

The results for cases AI and AII show that in the presence of significant amplitude small-scale mean fields and topography, the underestimation of small-scale kinetic energy that is characteristic of the Eulerian DIA closure (Herring *et al.* 1974; Frederiksen & Davies 2000), is reduced. This appears to be due to the fact that the quasi-diagonal approximation is then more successful in representing the off-diagonal elements of the two-point cumulants and this tends to offset the misrepresentation of the three-point cumulant by the Eulerian DIA. This may be seen from (3.6), where significant nonlinear noise and damping terms associated with eddy–mean field and eddy–topographic interactions may compensate for errors in the nonlinear noise and damping from eddy–eddy interactions. This compensation, as noted above, is most effective for case AII where the mean field kinetic energy spectrum is flatter. Then there is less difference between decay times determined by the mean field energy containing range and local excitation levels. This is confirmed by case BI where for strong small-scale topographic amplitude the small-scale kinetic energy and palinstrophy were found to compare very closely to DNS at moderate Reynolds number. Thus for the closure equations strong small-scale mean-field and topographic amplitudes result in increased verisimilitude.

The results of cases AI, AII & BI suggest that in the Eulerian QDIA the behaviour of the nonlinear damping and noise terms associated with eddy–mean field and eddy–topographic interactions results in the close comparison between DNS and CUQDIA closure fields at all scales despite the closure underestimating the evolved skewness. In cases where the flow is dominated by mean spectra that are nearly flat, then there is little difference between the local excitation levels and the energy containing range as far as determining de-correlation times in the equation for the two-time cumulant.

However, for cases at moderate and higher Reynolds numbers where the small-scale mean-field and topographic amplitudes are weak, it is expected, and subsequently confirmed, that the closure underestimates the evolved small scales in addition to more significant underestimation of the evolved skewness. These considerations led us to implement an empirical vertex renormalization procedure in which the eddy–mean field and eddy–topographic interactions, like the eddy–eddy transfer, are localized. This localization, or regularization as it has been termed by Frederiksen & Davies (2003), consists of zeroing the interaction coefficients $K(\boldsymbol{k}, \boldsymbol{p}, \boldsymbol{q})$ and $A(\boldsymbol{k}, \boldsymbol{p}, \boldsymbol{q})$ (2.4) in the two-time cumulant and response function equations unless the triad of interacting wave vectors satisfies certain inequalities depending on cutoff ratios α_1 and α_2.

The effectiveness of the regularization procedure in improving the small-scale amplitudes of kinetic energy and palinstrophy spectra for the CUQDIA closure has been tested for viscous decay of turbulence, starting from a variety of initial spectra. In particular two cases (BII and BIII) were studied at moderate large-scale Reynolds number ($R_L^{Case\ BII} \approxeq 200$ & $R_L^{Case\ BIII} \approxeq 300$) with the regularized closure performing very well. The findings have largely been presented for cutoff parameters $\alpha_1 = \alpha_2 = 4$, with the choice $\alpha_1 = 6, \alpha_2 = 3$ found to give very similar results in case BII.

For case BII, the initial conditions have mean and transient kinetic energy spectra that have broad similarities with atmospheric spectra. At large scales the mean kinetic energy dominates, while at small scales it is the transients and this remains the situation as the turbulence evolves to the final time ($t_f = 0.4$). The RCUQDIA closure, for both pairs of cutoff parameters, does a remarkable job in reproducing the evolved DNS kinetic energy and palinstrophy spectra, skewness and Reynolds number. This is in contrast to the CUQDIA closure, where mean and transient spectra have too small amplitude for $k > 20$ and the evolved skewness is less than 40% of the correct value. For this case we have also studied the sampling error in resolving the mean field when its magnitude is considerably less than the transients finding that an ensemble average of 1000 realizations was the minimum required to resolve the small-scale DNS mean field.

In case BIII we observe that the closure very accurately captures the early dynamics of the flow in a situation where there is rapid and significant transfer of energy from large to small scales and between mean and transient fields. Despite the very rapid evolution of the small-scale transients the regularized closure captures the evolution of the skewness and large-scale Reynolds number extremely accurately.

Our general results are also consistent with the DNS study of Bretherton & Haidvogel (1976), who found that in the presence of weak dissipation turbulent eddies over topography decay through a sequence of minimum enstrophy states for which the potential vorticity is proportional to the streamfunction. Carnevale & Frederiksen (1987) established the close relationship between minimum enstrophy states and canonical equilibrium states with maximum entropy. Holloway (1978) similarly found that for two-dimensional decaying topographic turbulence the mean vorticity flow was strongly anti-correlated to the topography with anti-cyclonic circulation around the hills and that after a period of strong development further energy transfer was suppressed and the mean and transient fields subsequently entered a period of steady decay.

In summary, we have performed a wide range of numerical experiments with the QDIA-type closures and shown that they are computationally tractable at reasonable resolutions in cumulant update form, and also accurate at very low to low Reynolds

numbers. At moderate Reynolds numbers, the QDIA closures tend to underestimate the magnitude of the small-scale transients, particularly for flows with weak mean fields and topographic amplitudes. This is related to inaccuracies in the representation of nonlinear noise and damping terms in the Eulerian QDIA associated with eddy–eddy, eddy–mean field and eddy–topographic interactions between large and small scales. These deficiencies can however be largely overcome by a regularized form of the CUQDIA closure in which transfers are localized in wavenumber space through specified cutoff parameters. We have found excellent agreement between a one-parameter form of the RCUQDIA closure and DNS results for turbulent flows with properties broadly similar to atmospheric spectra. This suggests that the regularized inhomogeneous QDIA closure may be sufficiently accurate to be applied to practical problems in geophysical fluids including the subgrid scale parameterization problem and the problem of predictability discussed in the Introduction.

A part of this work is based on a thesis submitted to Monash University and passed in fulfilment of the requirements for the degree of Doctor of Philosophy (O'Kane 2003). T. J. O. gratefully acknowledges the support of CSIRO Atmospheric Research, the Co-operative Research Center for Southern Hemisphere Meteorology, the School of Mathematics Monash University as well as a Monash University Graduate Award. T. J. O. also appreciates useful discussions with David J. Karoly.

Appendix A. Derivation of two-point restart terms

Let us now derive in detail the two-point restart terms using a perturbative approach. Suppose we expand $\hat{\zeta}_{\boldsymbol{k}}$ in a perturbation series

$$\hat{\zeta}_{\boldsymbol{k}}(t) = \hat{\zeta}^0_{\boldsymbol{k}}(t) + \lambda\hat{\zeta}^1_{\boldsymbol{k}}(t) + \ldots, \tag{A 1}$$

where the right-hand side terms are multiplied by the small expansion parameter λ. To zero order we have from (2.3)

$$\left(\frac{\partial}{\partial t} + \nu_0(k)k^2\right)\hat{\zeta}^0_{\boldsymbol{k}}(t) = \hat{f}^0_{\boldsymbol{k}}(t) + \delta(t-t_0)\hat{\zeta}^0_{\boldsymbol{k}}(t_0) \tag{A 2}$$

with formal solution in terms of the Green function $R^0_{\boldsymbol{k},\boldsymbol{k}}(t,s)$

$$\hat{\zeta}^0_{\boldsymbol{k}}(t) = R^0_{\boldsymbol{k},\boldsymbol{k}}(t,t_0)\hat{\zeta}^0_{\boldsymbol{k}}(t_0) + \int_{t_0}^{t} \mathrm{d}s\, R^0_{\boldsymbol{k},\boldsymbol{k}}(t,s)\hat{f}^0_{\boldsymbol{k}}(s). \tag{A 3}$$

To order λ we have

$$\begin{aligned}\left(\frac{\partial}{\partial t} + \nu_0(k)k^2\right)\hat{\zeta}^1_{\boldsymbol{k}}(t) \;=\; & \sum_{\boldsymbol{p}}\sum_{\boldsymbol{q}} \delta(\boldsymbol{k}+\boldsymbol{p}+\boldsymbol{q})A(\boldsymbol{k},\boldsymbol{p},\boldsymbol{q})\hat{\zeta}^0_{-\boldsymbol{p}}h_{-\boldsymbol{q}} \\ & + \sum_{\boldsymbol{p}}\sum_{\boldsymbol{q}} \delta(\boldsymbol{k}+\boldsymbol{p}+\boldsymbol{q})K(\boldsymbol{k},\boldsymbol{p},\boldsymbol{q})\left[\hat{\zeta}^0_{-\boldsymbol{p}}\hat{\zeta}^0_{-\boldsymbol{q}} - \left\langle\hat{\zeta}^0_{-\boldsymbol{p}}\hat{\zeta}^0_{-\boldsymbol{q}}\right\rangle\right] \\ & + \sum_{\boldsymbol{p}}\sum_{\boldsymbol{q}} \delta(\boldsymbol{k}+\boldsymbol{p}+\boldsymbol{q})\tfrac{1}{2}(A(\boldsymbol{k},\boldsymbol{p},\boldsymbol{q}) + A(\boldsymbol{k},\boldsymbol{q},\boldsymbol{p})) \\ & \times\left[\langle\zeta_{-\boldsymbol{p}}\rangle\hat{\zeta}^0_{-\boldsymbol{q}} + \langle\zeta_{-\boldsymbol{q}}\rangle\hat{\zeta}^0_{-\boldsymbol{p}}\right] + \delta(t-t_0)\hat{\zeta}^1_{\boldsymbol{k}}(t_0).\end{aligned} \tag{A 4}$$

Thus

$$\hat{\zeta}^1_{\boldsymbol{k}}(t) = \hat{\zeta}^{1(QDIA)}_{\boldsymbol{k}}(t) + R^0_{\boldsymbol{k},\boldsymbol{k}}(t,t_0)\hat{\zeta}^1_{\boldsymbol{k}}(t_0), \tag{A 5}$$

where

$$\hat{\zeta}_{\boldsymbol{k}}^{1(QDIA)}(t) = \int_{t_0}^{t} \mathrm{d}s\, R_{\boldsymbol{k},\boldsymbol{k}}^{0}(t,s)\Bigg[\sum_{\boldsymbol{p}}\sum_{\boldsymbol{q}}\delta(\boldsymbol{k}+\boldsymbol{p}+\boldsymbol{q})A(\boldsymbol{k},\boldsymbol{p},\boldsymbol{q})\hat{\zeta}_{-\boldsymbol{p}}^{0}(s)h_{-\boldsymbol{q}} + \sum_{\boldsymbol{p}}\sum_{\boldsymbol{q}}\delta(\boldsymbol{k}+\boldsymbol{p}+\boldsymbol{q})K(\boldsymbol{k},\boldsymbol{p},\boldsymbol{q})\big[\hat{\zeta}_{-\boldsymbol{p}}^{0}(s)\hat{\zeta}_{-\boldsymbol{q}}^{0}(s) - \big\langle\hat{\zeta}_{-\boldsymbol{p}}^{0}(s)\hat{\zeta}_{-\boldsymbol{q}}^{0}(s)\big\rangle\big] + \sum_{\boldsymbol{p}}\sum_{\boldsymbol{q}}\delta(\boldsymbol{k}+\boldsymbol{p}+\boldsymbol{q})\tfrac{1}{2}(A(\boldsymbol{k},\boldsymbol{p},\boldsymbol{q}) + A(\boldsymbol{k},\boldsymbol{q},\boldsymbol{p}))\big[\langle\zeta_{-\boldsymbol{p}}(s)\rangle\hat{\zeta}_{-\boldsymbol{q}}^{0}(s) + \langle\zeta_{-\boldsymbol{q}}(s)\rangle\hat{\zeta}_{-\boldsymbol{p}}^{0}(s)\big]\Bigg]. \tag{A 6}$$

We now similarly expand the two-time cumulant in a perturbation series

$$C_{\boldsymbol{k},-\boldsymbol{l}}^{QDIA}(t,t') = \langle\hat{\zeta}_{\boldsymbol{k}}(t)\hat{\zeta}_{-\boldsymbol{l}}(t')\rangle = \big\langle\hat{\zeta}_{\boldsymbol{k}}^{0}(t)\hat{\zeta}_{-\boldsymbol{l}}^{0}(t')\big\rangle + \lambda\big\langle\hat{\zeta}_{\boldsymbol{k}}^{1(QDIA)}(t)\hat{\zeta}_{-\boldsymbol{l}}^{0}(t')\big\rangle + \lambda\big\langle\hat{\zeta}_{\boldsymbol{k}}^{0}(t)\hat{\zeta}_{-\boldsymbol{l}}^{1(QDIA)}(t')\big\rangle + \ldots \tag{A 7}$$

Then assume that the initial $\hat{\zeta}_{\boldsymbol{k}}(t_0)$ have a multivariate Gaussian distribution, so that

$$\langle\hat{\zeta}_{\boldsymbol{k}}(t_0)\hat{\zeta}_{-\boldsymbol{l}}(t_0)\rangle = \delta_{\boldsymbol{k}\boldsymbol{l}}\langle\hat{\zeta}_{\boldsymbol{k}}(t_0)\hat{\zeta}_{-\boldsymbol{k}}(t_0)\rangle. \tag{A 8}$$

The further assumption of diagonal dominance imposes the following property on the zero order transient fields

$$\big\langle\hat{\zeta}_{\boldsymbol{k}}^{0}(t)\hat{\zeta}_{-\boldsymbol{l}}^{0}(t')\big\rangle = \delta_{\boldsymbol{k}\boldsymbol{l}}\big\langle\hat{\zeta}_{\boldsymbol{k}}^{0}(t)\hat{\zeta}_{-\boldsymbol{k}}^{0}(t')\big\rangle \tag{A 9}$$

so that to zero order

$$C_{\boldsymbol{k},-\boldsymbol{l}}^{0}(t,t') = \delta_{\boldsymbol{k}\boldsymbol{l}}\big\langle\hat{\zeta}_{\boldsymbol{k}}^{0}(t)\hat{\zeta}_{-\boldsymbol{k}}^{0}(t')\big\rangle, \tag{A 10}$$

to first order

$$C_{\boldsymbol{k},-\boldsymbol{l}}^{1(QDIA)}(t,t') = \big\langle\hat{\zeta}_{\boldsymbol{k}}^{1(QDIA)}(t)\hat{\zeta}_{-\boldsymbol{l}}^{0}(t')\big\rangle + \big\langle\hat{\zeta}_{\boldsymbol{k}}^{0}(t)\hat{\zeta}_{-\boldsymbol{l}}^{1(QDIA)}(t')\big\rangle \tag{A 11}$$

and

$$\begin{aligned} C_{\boldsymbol{k},-\boldsymbol{l}}^{1}(t,t') &= \big\langle\hat{\zeta}_{\boldsymbol{k}}^{1(QDIA)}(t)\hat{\zeta}_{-\boldsymbol{l}}^{0}(t')\big\rangle + \big\langle\hat{\zeta}_{\boldsymbol{k}}^{0}(t)\hat{\zeta}_{-\boldsymbol{l}}^{1(QDIA)}(t')\big\rangle \\ &\quad + R_{\boldsymbol{k},\boldsymbol{k}}^{0}(t,t_0)\big\langle\hat{\zeta}_{\boldsymbol{k}}^{1}(t_0)\hat{\zeta}_{-\boldsymbol{l}}^{0}(t')\big\rangle + R_{-\boldsymbol{l},-\boldsymbol{l}}^{0}(t',t_0)\big\langle\hat{\zeta}_{\boldsymbol{k}}^{0}(t)\hat{\zeta}_{-\boldsymbol{l}}^{1}(t_0)\big\rangle \\ &= \big\langle\hat{\zeta}_{\boldsymbol{k}}^{1(QDIA)}(t)\hat{\zeta}_{-\boldsymbol{l}}^{0}(t')\big\rangle + \big\langle\hat{\zeta}_{\boldsymbol{k}}^{0}(t)\hat{\zeta}_{-\boldsymbol{l}}^{1(QDIA)}(t')\big\rangle \\ &\quad + R_{\boldsymbol{k},\boldsymbol{k}}^{0}(t,t_0)R_{-\boldsymbol{l},-\boldsymbol{l}}^{0}(t',t_0)\big\langle\hat{\zeta}_{\boldsymbol{k}}^{1}(t_0)\hat{\zeta}_{-\boldsymbol{l}}^{0}(t_0)\big\rangle \\ &\quad + R_{\boldsymbol{k},\boldsymbol{k}}^{0}(t,t_0)R_{-\boldsymbol{l},-\boldsymbol{l}}^{0}(t',t_0)\big\langle\hat{\zeta}_{\boldsymbol{k}}^{0}(t_0)\hat{\zeta}_{-\boldsymbol{l}}^{1}(t_0)\big\rangle \\ &= \big\langle\hat{\zeta}_{\boldsymbol{k}}^{1(QDIA)}(t)\hat{\zeta}_{-\boldsymbol{l}}^{0}(t')\big\rangle + \big\langle\hat{\zeta}_{\boldsymbol{k}}^{0}(t)\hat{\zeta}_{-\boldsymbol{l}}^{1(QDIA)}(t')\big\rangle \\ &\quad + R_{\boldsymbol{k},\boldsymbol{k}}^{0}(t,t_0)R_{-\boldsymbol{l},-\boldsymbol{l}}^{0}(t',t_0)C_{\boldsymbol{k},-\boldsymbol{l}}(t_0,t_0) \\ &= C_{\boldsymbol{k},-\boldsymbol{l}}^{1(QDIA)}(t,t') + R_{\boldsymbol{k},\boldsymbol{k}}^{0}(t,t_0)R_{-\boldsymbol{l},-\boldsymbol{l}}^{0}(t',t_0)C_{\boldsymbol{k},-\boldsymbol{l}}(t_0,t_0). \end{aligned} \tag{A 12}$$

We now renormalize (A 12); that is $\lambda \to 1$, $R_{\boldsymbol{k},\boldsymbol{k}}^{0} \to R_{\boldsymbol{k},\boldsymbol{k}}$, $C_{\boldsymbol{k},-\boldsymbol{k}}^{0} \to C_{\boldsymbol{k},-\boldsymbol{k}}$ and $C_{\boldsymbol{k},-\boldsymbol{l}}^{1} \to C_{\boldsymbol{k},-\boldsymbol{l}}$ with $C_{\boldsymbol{k},-\boldsymbol{l}}(t_0,t_0) = \langle\hat{\zeta}_{\boldsymbol{k}}(t_0)\hat{\zeta}_{-\boldsymbol{l}}(t_0)\rangle$. Thus we have for $t \geqslant t' \geqslant T$

$$C_{\boldsymbol{k},-\boldsymbol{l}}(t,t') = \int_{T}^{t} \mathrm{d}s\; R_{\boldsymbol{k},\boldsymbol{k}}(t,s)C_{-\boldsymbol{l},\boldsymbol{l}}(t',s)[A(\boldsymbol{k},-\boldsymbol{l},\boldsymbol{l}-\boldsymbol{k})h_{\boldsymbol{k}-\boldsymbol{l}} + (A(\boldsymbol{k},-\boldsymbol{l},\boldsymbol{l}-\boldsymbol{k}) + A(\boldsymbol{k},\boldsymbol{l}-\boldsymbol{k},-\boldsymbol{l}))\langle\zeta_{\boldsymbol{k}-\boldsymbol{l}}(s)\rangle]$$

$$+\int_T^{t'} \mathrm{d}s\, C_{\boldsymbol{k},-\boldsymbol{k}}(t,s)R_{-\boldsymbol{l},-\boldsymbol{l}}(t',s)[A(-\boldsymbol{l},\boldsymbol{k},\boldsymbol{l}-\boldsymbol{k})h_{\boldsymbol{k}-\boldsymbol{l}}$$
$$+(A(-\boldsymbol{l},\boldsymbol{k},\boldsymbol{l}-\boldsymbol{k})+A(-\boldsymbol{l},\boldsymbol{l}-\boldsymbol{k}),\boldsymbol{k})\langle\zeta_{\boldsymbol{k}-\boldsymbol{l}}(s)\rangle]$$
$$+R_{\boldsymbol{k},\boldsymbol{k}}(t,T)R_{-\boldsymbol{l},-\boldsymbol{l}}(t',T)C_{\boldsymbol{k},-\boldsymbol{l}}(T,T),$$
$$=C^{(QDIA)}_{\boldsymbol{k},-\boldsymbol{l}}(t,t')+R_{\boldsymbol{k},\boldsymbol{k}}(t,T)R_{-\boldsymbol{l},-\boldsymbol{l}}(t',T)C_{\boldsymbol{k},-\boldsymbol{l}}(T,T). \tag{A 13}$$

For $t=t'=T$, using the reduced notation of (3.2*b*) and a reordering of the wavevectors, we find that

$$C_{-\boldsymbol{p},-\boldsymbol{k}}(T,T)=\int_{t_0}^{T}\mathrm{d}s\, R_{-\boldsymbol{p}}(T,s)C_{-\boldsymbol{k}}(T,s)\big[A(-\boldsymbol{p},-\boldsymbol{k},\boldsymbol{k}+\boldsymbol{p})h_{(-\boldsymbol{k}-\boldsymbol{p})}+(A(-\boldsymbol{p},-\boldsymbol{k},\boldsymbol{k}+\boldsymbol{p})$$
$$+A(-\boldsymbol{p},\boldsymbol{k}+\boldsymbol{p},-\boldsymbol{k}))\big\langle\zeta_{(-\boldsymbol{k}-\boldsymbol{p})}(s)\big\rangle\big]+\int_{t_0}^{T}\mathrm{d}s\, R_{-\boldsymbol{k}}(T,s)C_{-\boldsymbol{p}}(T,s)$$
$$\times\big[A(-\boldsymbol{k},-\boldsymbol{p},\boldsymbol{k}+\boldsymbol{p})h_{(-\boldsymbol{k}-\boldsymbol{p})}+(A(-\boldsymbol{k},-\boldsymbol{p},\boldsymbol{k}+\boldsymbol{p})+A(-\boldsymbol{k},\boldsymbol{k}$$
$$+\boldsymbol{p},-\boldsymbol{p}))\big\langle\zeta_{(-\boldsymbol{k}-\boldsymbol{p})}(s)\big\rangle\big]+R_{-\boldsymbol{p}}(T,t_0)R_{-\boldsymbol{k}}(T,t_0)C_{-\boldsymbol{p},-\boldsymbol{k}}(t_0,t_0), \tag{A 14}$$

which is equivalent to (3.10*a*), namely

$$\tilde{K}^{(2)}_{-\boldsymbol{p},-\boldsymbol{k}}(T,T)=K^{(2)Dyn}_{-\boldsymbol{p},-\boldsymbol{k}}(T,T)+\tilde{K}^{(2)}_{-\boldsymbol{p},-\boldsymbol{k}}(t_0,t_0)R_{-\boldsymbol{p}}(T,t_0)R_{-\boldsymbol{k}}(T,t_0), \tag{A 15}$$

where $K^{(2)Dyn}_{-\boldsymbol{p},-\boldsymbol{k}}(t,t')=C^{(QDIA)}_{-\boldsymbol{p},-\boldsymbol{k}}(t,t')$.

REFERENCES

Alvarez, A., Tintore, J., Holloway, G., Eby, M. & Beckers J. M. 1994 Effect of topographic stress on circulation in the western Mediterranean. *J. Geophys. Res.* **99**, 16053–16064.

Boffetta, G., Celani, A., Crisanti, A. & Vulpiani, A. 1997 Predictability in two-dimensional deacying turbulence. *Phys. Fluids* **9**, 724–734.

Boer, G. J. & Shepherd, T. G. 1983 Large-scale two-dimensional turbulence in the atmosphere. *J. Atmos. Sci.* **40**, 164–184.

Bowman, J. C., Krommes, J. A. & Ottaviani, M. 1993 The realizable Markovian closure. I. General theory, with applications to 3-wave dynamics. *Phys. Fluids* **5**, 3558–3589.

Bowman, J. C. & Krommes, J. A. 1997 The realizable Markovian closure and realizable test-field model. II. Application to anisotropic drift-wave dynamics. *Phys. Plasmas* **4**, 3895–3909.

Bretherton, F. P. & Haidvogel, D. B. 1976 Two-dimensional turbulence above topography. *J. Fluid Mech.* **78**, 129–154.

Carnevale, G. F. & Frederiksen, J. S. 1987 Nonlinear stability and statistical mechanics of flow over topography. *J. Fluid Mech.* **175**, 157–181.

Carnevale, G. F. & Martin, P. C. 1982 Field theoretical techniques in statistical fluid dynamics: with applications to nonlinear wave dynamics. *Geophys. Astrophys. Fluid Dyn.* **20**, 131–164.

Carnevale, G. F., Purini, R., Orlandi, P. & Cavazza, P. 1995 Barotropic quasi-geostrophic f-plane flow over anisotropic topography. *J. Fluid Mech.* **285**, 329–347.

Chasnov, J. R. 1991 Simulation of the Kolmogorov inertial subrange using an improved subgrid model. *Phys. Fluids* A **3**, 188–200.

Frederiksen, J. S. 1982 Eastward and westward flows over topography in nonlinear and linear barotropic models. *J. Atmos. Sci.* **39**, 2477–2489.

Frederiksen, J. S. 1999 Subgrid-scale parameterizations of eddy–topographic force, eddy viscosity, and stochastic backscatter for flow over topography. *J. Atmos. Sci.* **56**, 1481–1494.

Frederiksen, J. S., Collier, M. A. & Watkins, A. B. 2002 Ensemble prediction methods based on fast growing perturbations. *CSIRO Atmospheric Research Technical Paper* No. 59, pp. 1–27. http://www.dar.csiro.au/publications/frederiksen_2002a.pdf

Frederiksen, J. S. & Davies, A. G. 1997 Eddy viscosity and stochastic backscatter parameterizations on the sphere for atmospheric circulation models. *J. Atmos. Sci.* **54**, 2475–2492.

Frederiksen, J. S. & Davies, A. G. 2000 Dynamics and spectra of cumulant update closures for two-dimensional turbulence. *Geophys. Astrophys. Fluid Dyn.* **92**, 197–231.

Frederiksen, J. S. & Davies, A. G. 2003 The regularized DIA closure for two-dimensional turbulence. *Geophys. Astrophys. Fluid Dyn.* (in press).

Frederiksen, J. S., Davies, A. G. & Bell, R. C. 1994 Closure equations with non-Gaussian restarts for truncated two-dimensional turbulence. *Phys. Fluids* **6**, 3153–3163.

Frederiksen, J. S., Dix, M. R. & Davies, A. G. 2003 The effects of closure-based eddy diffusion on the climate and spectra of a GCM. *Tellus* **55A**, 31–44.

Frederiksen, J. S. & Sawford, B. L. 1980 Statistical dynamics of two-dimensional inviscid flow on a sphere. *J. Atmos. Sci.* **37**, 717–732.

Gotoh, T., Kaneda, Y. & Bekki, N. 1988 Numerical integration of the Lagrangian Renormalized Approximation. *J. Phys. Soc. Japan* **57**, 866–880.

Herring, J. R. 1965 Self-consistent-field approach to turbulence theory. *Phys. Fluids* **8**, 2219–2225.

Herring, J. R. 1977 On the statistical theory of two-dimensional topographic turbulence. *J. Atmos. Sci.* **34**, 1731–1750.

Herring, J. R., Orszag, S. A., Kraichnan, R. H. & Fox, D. G. 1974 Decay of two-dimensional homogeneous turbulence. *J. Fluid Mech.* **66**, 417–444.

Herring, J. R. & Kraichnan, R. H. 1979 A numerical comparison of velocity-based and strain based Lagrangian-history turbulence approximations. *J. Fluid Mech.* **91**, 581–597.

Holloway, G. 1978 A spectral theory of nonlinear barotropic motion above irregular topography. *J. Phys. Oceanogr.* **8**, 414–427.

Holloway, G. 1992 Representing topographic stress for large-scale ocean models. *J. Phys. Oceanogr.* **22**, 1033–1046.

Jensen, R. V. 1981 Functional integral approach to classical statistical dynamics. *J. Statist. Phys.* **25**, 183–210.

Kells, L. C. & Orszag, S. A. 1978 Randomness of low-order models of two-dimensional inviscid dynamics. *Phys. Fluids* **21**, 162–168.

Kraichnan, R. H. 1958 Irreversible statistical mechanics of incompressible hydrodynamic turbulence. *Phys. Rev.* **109**, 1407–1422.

Kraichnan, R. H. 1959 The structure of isotropic turbulence at very high Reynolds numbers. *J. Fluid Mech.* **5**, 497–543.

Kraichnan, R. H. 1964*a* Decay of isotropic turbulence in the direct interaction approximation. *Phys. Fluids* **7**, 1030–1048.

Kraichnan, R. H. 1964*b* Diagonalizing approximation for inhomogeneous turbulence. *Phys. Fluids* **7**, 1169–1177.

Kraichnan, R. H. 1964*c* Kolmogorov's hypothesis and Eulerian turbulence theory. *Phys. Fluids* **7**, 1723–1734.

Kraichnan, R. H. 1970 Instability in fully developed turbulence. *Phys. Fluids* **13**, 569–575.

Kraichnan, R. H. 1971*a* An almost-Markovian Galilean-invariant turbulence model. *J. Fluid Mech.* **47**, 513–524.

Kraichnan, R. H. 1971*b* Inertial-range transfer in two and three dimensional turbulence. *J. Fluid Mech.* **47**, 525–535.

Kraichnan, R. H. 1972 Test-field model for inhomogeneous turbulence. *J. Fluid Mech.* **56**, 287–304.

Kraichnan, R. H. 1976 Eddy viscosity in two and three dimensions. *J. Atmos. Sci.* **33**, 1521–1536.

Kraichnan, R. H. 1977 Eulerian and Lagrangian renormalization in turbulence theory. *J. Fluid Mech.* **83**, 349–374.

Lee, L. L. 1965 A formulation of the theory of isotropic hydromagnetic turbulence in an incompressible fluid. *Annal. Phys.* **32**, 292–321.

Leith, C. E. 1971 Atmospheric predictability and two-dimensional turbulence. *J. Atmos. Sci.* **28**, 145–161.

Leith, C. E. 1974 Theoretical skill of Monte Carlo forecasts. *Mon. Wea. Rev.* **102**, 409–418.

Leith, C. E. 1990 Stochastic backscatter in a subgrid-scale model: Plane shear mixing layer. *Phys. Fluids* A **2**, 297–299.

Leith, C. E. & Kraichnan, R. H. 1972 Predictability of turbulent flows. *J. Atmos. Sci.* **29**, 1041–1058.

Leslie, D. C. 1973 *Developments in the Theory of Turbulence*. Clarendon.

Lorenz, E. N. 1969 The predictability of a flow which possesses many scales of motion. *Tellus* **21**, 289–307.

Martin, P. C., Siggia, E. D. & Rose, H. A. 1973 Statistical dynamics of classical systems. *Phys. Rev.* A **8**, 423–437.

McComb, W. D. 1974 A local energy-transfer theory of isotropic turbulence. *J. Phys.* A **7**, 632–649.

McComb, W. D. 1990 *The Physics of Fluid Turbulence*. Clarendon.

McComb, W. D., Filipiak, M. J. & Shanmugasundaram, V. 1992 Rederivation and further assesment of the LET theory of isotropic turbulence, as applied to passive scalar convection. *J. Fluid Mech.* **245**, 279–300.

McComb, W. D. & Quinn, A. P. 2003 Two-point two-time closures applied to forced isotropic turbulence. *Physica* A **317**, 487–508.

McWilliams, J. C. 1984 The emergence of isolated coherent vorticies in turbulent flow. *J. Fluid Mech.* **146**, 21–43.

O'Kane, T. J. 2003 The statistical dynamics of geophysical flows: an investigation of two-dimensional turbulent flow over topography. PhD thesis, Monash University, Australia.

Orszag, S. A. 1970 Analytical theories of turbulence. *J. Fluid Mech.* **41**, 363–386.

Orszag, S. A. 1973 Statistical theories of turbulence. In *Les Houches Summer School of Theoretical Physics, Fluid Dynamics 1973* (ed. R. Balian and J.-L. Peube) pp. 235–374. Gordon and Breach.

Phythian, R. 1975 The operator formalism of classical statistical dynamics. *J. Phys.* A **8**, 1423–1432.

Rose, H. A. 1977 Eddy diffusivity, eddy noise and subgrid-scale modeling. *J. Fluid Mech.* **81**, 719–734.

Rose, H. A. 1985 An efficient non-Markovian theory of non-equilibrium dynamics. *Physica* D **14**, 216–226.

Schilling, O. & Zhou, Y. 2002 Analysis of spectral eddy viscosity and backscatter in incompressible, isotropic turbulence using statistical closure theory. *Phys. Fluids* **14**, 1244–1258.

Toth, Z. & Kalnay, E. 1997 Ensemble forecasting at NCEP and the breeding method. *Mon. Wea. Rev.* **125**, 3297–3319.

Wyld, H. W. 1961 Formulation of the theory of turbulence in an incompressible fluid. *Ann. Phys.* **14**, 143–165.